RESEARCH ON A NEW TYPE OF NEGATIVE HYDROGEN ION SOURCE

FINAL REPORT

FOR

AFOSR-81-0160
United States Air Force
Air Force Office of Scientific Research
Building 410
Bolling AFB, D.C. 20332

AD-A170 068

MAY 1986

Prepared by

R. J. Turnbull
Department of Electrical and Computer Engineering
University of Illinois
Urbana, IL 61801

"The views and conclusions contained in this document are those of the author
and should not be interpreted as necessarily representing the official policies
or endorsements, either expressed or implied, of the Air Force Office of
Scientific Research or the U.S. Government."

86 7 23 091

TABLE OF CONTENTS

86 7   23 091

REPORT DOCUMENTATION PAGE	READ INSTRUCTIONS BEFORE COMPLETING FORM
1. REPORT NUMBER AFOSR-TR. 86-0476	2. GOVT ACCESSION NO. AD-A170068	3. RECIPIENT'S CATALOG NUMBER

4. TITLE (and Subtitle) RESEARCH ON A NEW TYPE OF NEGATIVE HYDROGEN ION SOURCE	5. TYPE OF REPORT & PERIOD COVERED FINAL REPORT 15 July 1981 to 14 Jan. 1985
	6. PERFORMING ORG. REPORT NUMBER

7. AUTHOR(s) R. J. Turnbull	8. CONTRACT OR GRANT NUMBER(s) AFOSR-81-0160

9. PERFORMING ORGANIZATION NAME AND ADDRESS Fusion Technology Laboratory, Dept. of Elec. Eng. University of Illinois, 1406 W. Green Street Urbana, IL 61801	10. PROGRAM ELEMENT, PROJECT, TASK AREA & WORK UNIT NUMBERS 61102F 2301/A7

11. CONTROLLING OFFICE NAME AND ADDRESS United States Air Force Air Force Office of Scientific Research Building 40, Bolling AFB, DC 20332	12. REPORT DATE 19 May 1986
	13. NUMBER OF PAGES 60

14. MONITORING AGENCY NAME & ADDRESS(if different from Controlling Office)	15. SECURITY CLASS. (of this report) UNCLASSIFIED
	15a. DECLASSIFICATION/DOWNGRADING SCHEDULE

16. DISTRIBUTION STATEMENT (of this Report)

Distribution Unlimited

Approved for public release;
distribution unlimited.

17. DISTRIBUTION STATEMENT (of the abstract entered in Block 20, if different from Report)

DTIC
ELECTE
JUL 2 4 1986
S   D
D

18. SUPPLEMENTARY NOTES

19. KEY WORDS (Continue on reverse side if necessary and identify by block number)

Ion source, neutral beams, negative hydrogen ions.

20. ABSTRACT (Continue on reverse side if necessary and identify by block number)

The production of negative hydrogen ions in a discharge is greatly enhanced if the hydrogen is vibrationally excited. In the work presented here is a study of a method of producing vibrationally excited hydrogen. The technique used is to heat dense hydrogen hot enough to produce vibrational excitation and then allow it to expand thus cooling it while maintaining the vibrational excitation. Both theoretical calculations and experimental results on this technique are presented.

DD FORM 1473
1 JAN 73

RESEARCH OBJECTIVES

The objective of this research is to produce negative hydrogen ion by: heating hydrogen so that it is vibrationally excited; allowing it to expand under conditions that its translational temperature drops but its vibrational excitation remains; and formation of negative ions in a discharge by dissociative attachment on vibrationally excited H_2. The initial heating is to be done by laser heating of solid hydrogen or discharge heating of high pressure hydrogen gas.

STATUS OF THE RESEARCH EFFORT

I.   Theory of Production of Vibrationally Excited Hydrogen for
      use in a Negative Ion Source

INTRODUCTION

The generation of negative hydrogen (or deuterium) ions in a
volume process is due mostly to the dissociative attachment process.
In this process an electron impacts a molecule producing a negative
ion and a neutral atom. In hydrogen the cross section for this
process increases by five orders of magnitude as the molecule is
raised from the ground state to the fifth vibrationally excited
state. In addition the peak of the cross-section occurs at a lower
energy thus allowing a larger fraction of the electrons in a
discharge to undergo the reaction. If the molecular hydrogen in a
discharge is vibrationally excited the production of negative
hydrogen can be greatly enhanced. (In deuterium the effect of
vibrational excitation on the cross-section is even more pronounced.)
This research is designed to test if negative hydrogen ion
production can be enhanced by producing vibrationally excited
hydrogen and flowing it through an electrical discharge. In the next
section the proposed source is described. Then predictions from
theoretical calculations are presented. Finally, results from two
experiments designed to produce vibrationally excited hydrogen are
presented.

PRODUCTION TECHNIQUE

The negative ion source envisioned in this work is a three-stage
device as shown in Figure 1. In the first stage dense hydrogen is
heated to a temperature such that an appreciable fraction of it is
vibrationally excited. In the second stage the hydrogen gas expands

and cools while maintaining its vibrationally excited state and the
final stage is a discharge through which the gas flows producing
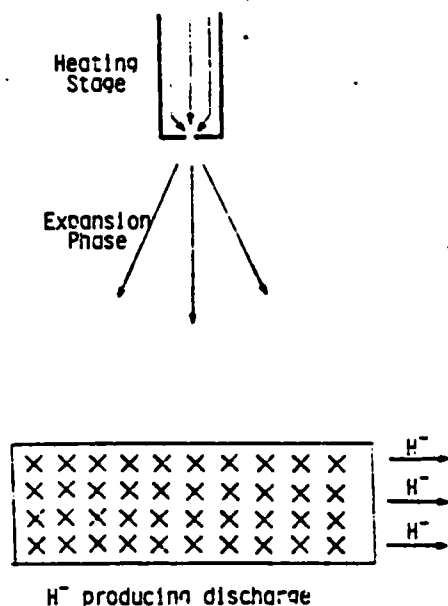negative hydrogen.

Figure 1. Negative Ion Source
Using Pre-Discharge Vibrational
Excitation of the Hydrogen

In order to produce vibrationally excited hydrogen by heating, it is necessary to use a dense gas because at the temperatures needed to produce a high excited fraction most of the hydrogen will be dissociated if the gas is not dense (several atmospheres or better). The excited and dissociated fraction can be calculated from equilibrium equations since equilibrium is established rapidly in a dense medium. The heating can be done either by an electrical discharge in the gas as shown in Figure 1 or by a laser on a small solid hydrogen sample. Both techniques will be discussed in later sections of this paper.

The expansion will be flow out of a nozzle if the heating is done by a discharge or free expansion if the heating done by a laser on a solid. As the gas expands it cools with the degree of cooling calculated using isentropic expansion equations. If the mass flow rate is not too large the time needed for the vibrational energy to be converted to translational energy is long compared to the flow time and the molecules remain excited. Calculations in the next section will illustrate this.
The negative ion forming discharge stage will be treated in a later paper.

THEORETICAL CALCULATIONS

Calculations were done on the flow expansion to determine the
resulting level of vibrational excitation and the resulting negative
ion formation rate. A hot dense gas in thermal equilibrium is
allowed to expand. As it expands collisions between molecules result
in vibrational-to-translational energy transfers as well as
vibrational-vibrational energy transfers. Because of the anharmonic
nature of the vibrational energy levels and because the higher levels
(4-6) are extremely important in negative ion production, it was
necessary to calculate the population of each level separately rather
than assume a vibrational temperature. The resulting populations of
the vibrational levels were calculated using a Runge-Kutta technique
and the results were shown to depend on the initial temperature

(T_0) and the product of the initial density and the radius of the nozzle from which the gas emerged(nr). Results are shown in Figure 2. In Fig.(2a) the initial temperature was 3000 K and in Fig.(2b) the initial temperature was 5000 K. The equilibrium populations are shown as well as the populations after the expansion takes place. The density times radius units are in cm^{-2}. From this graph it is seen that the higher levels tend to depopulate more than the lower levels. A density radius product of about 10^{18} cm^{-2} is about the upper limit which preserves most of the vibrational excitation. Above that most of the vibrational energy is converted to translational energy.

(a)

EXPANSION WITH T0=3000

(b)

EXPANSION WITH T0=5000

* NR=1E17
* NR=1E18
* NR=1E19
* NR=1E20
* EQUIL
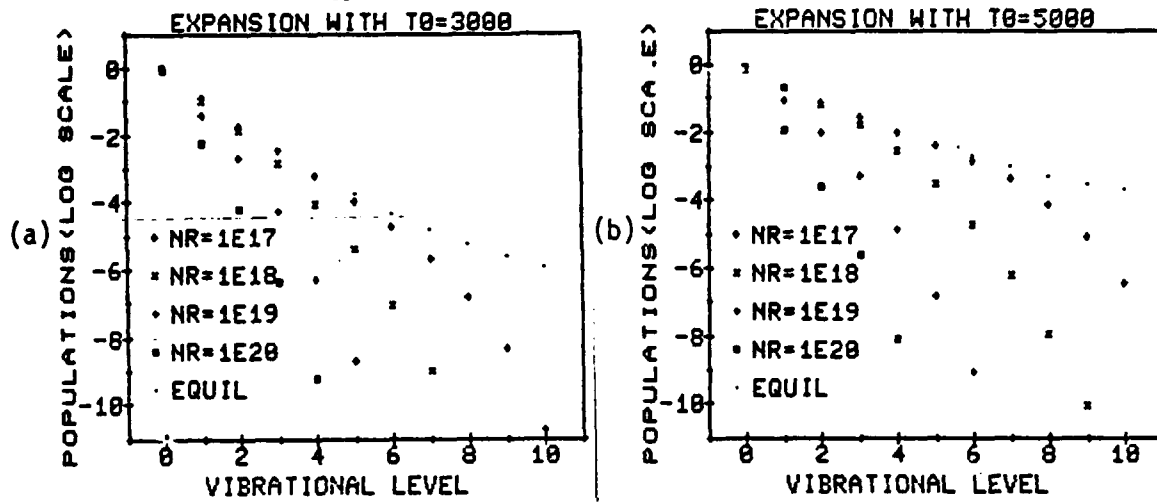
Figure 2. Vibrational State Populations Resulting from Expansion of a Heated Gas. (a) Initial Temperature - 3000 K; (b) Initial Temperature - 5000 K.

ANHARMONIC PUMPING
TV=4000 NT=1E14

* T=100
* T=200
* T=300
* EQUIL
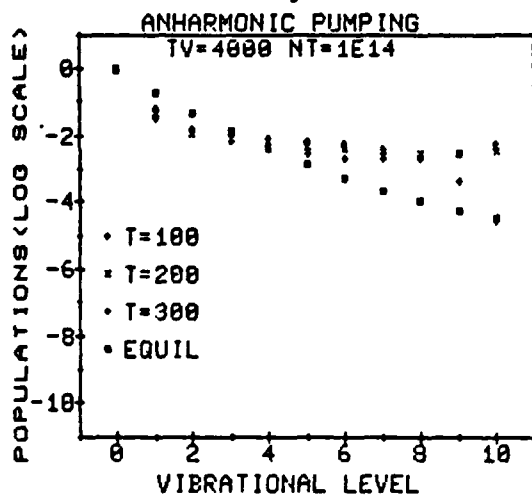
Figure 3. Enhancement of Higher Vibrational State Population by Anharmonic Pumping

An effect which does not appear to be important in the expansion is anharmonic pumping. This phenomena occurs in a cool gas with a large vibrational energy. Because of the anharmonic nature of the vibrational levels the energy tends to go into the higher states populating them higher than would be expected if the levels were in equilibrium. Calculations were also done on this effect assume a starting point a gas with a vibrational equilibrium at a much higher temperature than the translational temperature. The density was assumed constant and some results are shown in Figure

3 with an initial vibrational temperature of 4000 K and translational temperatures of a few hundred degrees. (The results are similar to those of Reference 1 which uses this effect in a proposed source.) A product of density and time (nt) equal to 10^{14} cm^{-3}-sec was needed to see an appreciable effect. As translational temperatures are raised anharmonic pumping becomes less important.

In order to determine if negative ion production can be enhanced by this technique, the vibrational populations calculated from the expansion were assumed to go into a discharge of 40 Townsend (Tn) and the resulting negative ion production rates were calculated. The electron distributed was calculated using the upflux method of Reference 2. This is shown in Figure 4 for various initial temperatures and density-radius products. An nr product of 10^{17} cm^{-2} produces results close to those of equilibrium vibration populations at the given temperature while an nr of 10^{20} cm^{-2} gives results similar to unexcited H_2. Enhancement of H$^-$ production rates of 100-1000 are predicted here. For the purposes of comparison Figure 5 is presented. It shows H$^-$ production rates which result taking into account the vibrational excitation which takes place in a discharge. It shows that a product of electron density times time of $\sim 10^8$ cm^3-sec is necessary to reach the same H$^-$ production rates as the heated expansion.

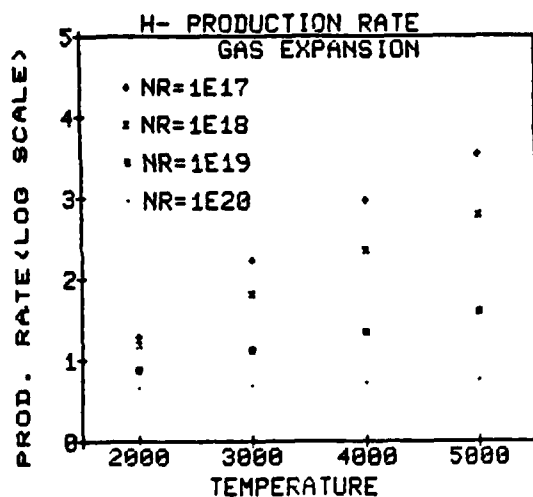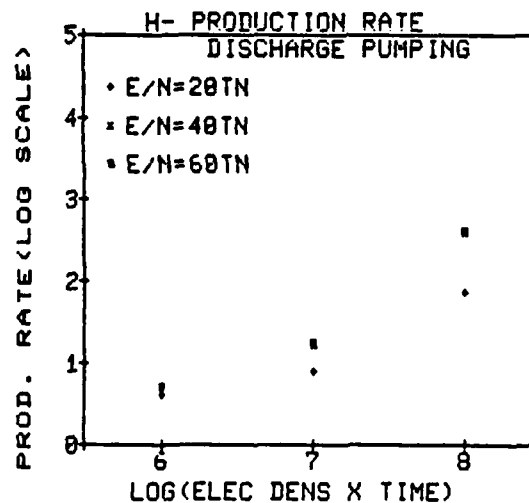Figure 4. Negative Hydrogen Ion Production Rates for Vibrational Excited Hydrogen Produced by the Expansion Process

Figure 5. Negative Hydrogen Ion Production Rate from Discharge Pumping of Hydrogen Vibrational States

REFERENCES

1) A. Garscadden and W. F. Bailey, Progress in Astronautics and

Aeronautics, Vol. 74, p. 1125, 1980.

2) W. P. Allis and H. A. Haus, J. Appl. Phys., 45, 781 (1974).

Indirect heating of solid hydrogen with a moderately powered laser

J. L. Guttman[a] and R. J. Turnbull

Department of Electrical Engineering, University of Illinois, Urbana, Illinois 61801

In this paper we describe experiments in which solid hydrogen is heated by laser-produced plasma. Motivation for this experiment is the possibility of producing large quantities of vibrationally excited hydrogen. (Vibrationally excited hydrogen is desirable for the production of H^- ions by dissociative attachment.) A possible technique for formation of vibrationally excited hydrogen is heating it to 3000–5000 K in a dense enough state so that little dissociation takes place. The heated hydrogen is then allowed to expand and cool but because of a long relaxation time for deexcitation the vibrational excitation persists. A thin slab of solid hydrogen was mounted on a metal substrate, and laser light with power density 10^8–10^9 W/cm^2 was used to heat the target. Because of the desired temperature the hydrogen could not be heated directly. (This would require much larger laser power which, in turn, would heat the hydrogen to much too high a temperature.) The laser light was absorbed by the metal substrate, and the resulting plasma transferred its energy to the solid hydrogen. Experimental results to determine resulting hydrogen temperatures are presented for different slab thicknesses. Diagnostics used included fast-framing and streak photography, Faraday cups, and a piezoelectric probe. A model is developed which allows the results to be explained. Hydrogen is ablated off the slab at the metal plasma surface, and the gas is heated by heat transfer. A shock wave is driven into the hydrogen. Then depending on the slab thickness one of two things occurs. For thin slabs we propose a Rayleigh-Taylor instability which causes the hydrogen to blow a hole in the solid (or liquid) and expand into vacuum. Under the right condition the expanded gas can then be used for H^- production. If the slab is too thick, the shock wave becomes strong enough to produce vaporization. The resulting gas mixes with the heated gas, cooling it and preventing any large amount of vibrational excitation.

I. INTRODUCTION

Intense high-energy neutral hydrogen beams may be used for heating magnetic fusion plasmas as well as for other uses. At high energies (> 150 keV) negative hydrogen (H^-) ions are required for efficient production of neutral beams because negative ions are easier to neutralize.[1] One method of producing H^- is the direct extraction of H^- ions formed in hydrogen discharge plasmas. The dominant mechanism for creation of H^- ions in these plasmas is dissociative attachment of electrons to vibrationally excited hydrogen molecules.[2] Therefore, by enhancing the percentage of vibrationally excited molecules in a hydrogen discharge source, the H^- ion yield should increase.

We have investigated a technique for producing large quantities of vibrationally excited hydrogen molecules. The production of vibrationally excited hydrogen is based on the following physics. The equilibrium fraction of hydrogen gas which is in the form of vibrationally excited molecules depends on the temperature of the gas and on the dissociated fraction. (If the hydrogen is dissociated, it cannot be vibrationally excited.) The dissociated fraction depends on both temperature and density, with the fraction at a given temperature decreasing with increasing density. In order to have a large fraction of vibrationally excited molecules at equilibrium, the temperature and density must be such that only a

small fraction are dissociated. From equilibrium population calculations for hydrogen for densities ranging from 10^{19} to 10^{22} atoms/cm^3, the optimum vibrationally excited fraction occurs at temperatures ranging from 3000 to 6000 K.[3] (Solid density is about 5×10^{22} atoms/cm^3.)

If a volume of solid hydrogen is suddenly heated to a high temperature while the surrounding volume is either vacuum or low-pressure gas, the hydrogen will undergo free expansion. The velocity of expansion will be approximately the sonic velocity at the temperature immediately after heating. A qualitative description of the flow is the following. Since the hydrogen is expanding into vacuum, the expansion will be supersonic with the temperature and density both decreasing with increasing radius. Directly after heating, the vibrational excitation is in equilibrium with the translational and rotational motion because of the high density. However, as the radius increases, the density and temperature decrease, causing the vibrational relaxation time to increase rapidly.[4] (The vibrational relaxation time is the time needed to establish equilibrium between vibrational and translational energy. This requires a large number of collisions.) When this time becomes long compared to the time needed for the translational temperature to change substantially, the vibrational excitation is no longer coupled to the flow and the vibrational states "freeze." That is, to a good approximation, beyond this point no more vibrational deexcitation takes place. The temperature at this freezing point determines the fraction of molecules which are still vibrationally excited. In particular, if the density and temperature at the freezing point are in the range of values mentioned previous-

[a] Current address: Lockheed Palo Alto Research, 3251 Hanover Street, Department 52-11 Building 203, Palo Alto, California 94304.
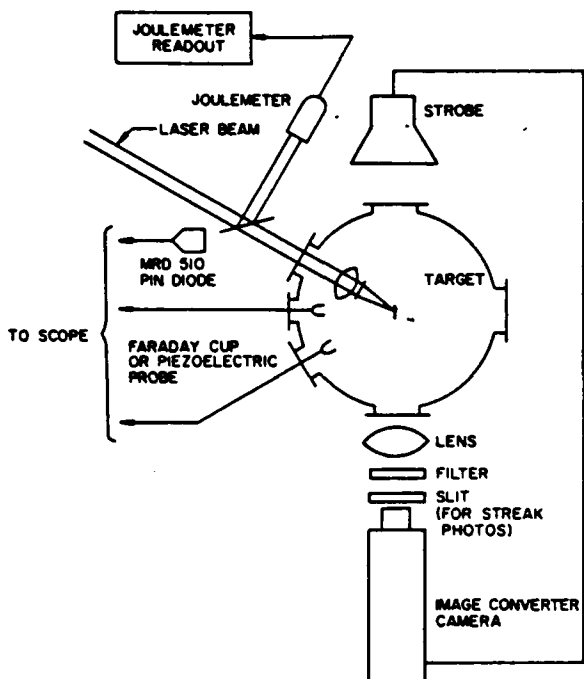
FIG. 1. Experimental setup for laser heating of hydrogen.

FIG. 2. Laser beam temporal profile.

ly, the fraction of vibrationally excited molecules in the ex-
˜ded gas will be large.

In summary, the technique involves rapidly heating a
volume of solid hydrogen and letting it expand into vacuum.
If the flow conditions are right, a nonequilibrium population
of vibrationally excited molecules will exist. Ultimately, a
flow of this type would be used in conjunction with an elec-
tric discharge to provide a source of H^- ions.

This paper addresses the heating aspect of this source,
using a pulsed red-dye laser. Note that the laser irradiance
must be below the breakdown threshold for solid hydrogen
(10^{10} W/cm^2), because ionized hydrogen is not desired.
However, we have observed in our laboratory that solid hy-
drogen is transparent to red laser irradiance in the 10^8–10^9
W/cm^2 range. Consequently, it is necessary to heat the solid
hydrogen indirectly. This is accomplished by positioning a
slab of solid hydrogen against a metallic substrate. The laser
beam incident on the slab passes through it and is absorbed
at the substrate surface. The hydrogen is then heated by heat
transfer from the resulting metal plasma.

The experimental apparatus will be described in the
next section, followed in succeeding sections by the experi-
mental results and a model which explains the results and
allows an optimum system to be designed.

II. EXPERIMENTAL APPARATUS

The experimental setup is shown in Fig. 1. The laser
used in this experiment is a flashlamp pumped dye laser with
Rhodamine 6G dye. The maximum output energy is 4 J with
full-width half-maximum pulse width of approximately 600
ns and beam diameter approximately 1.8 cm. The laser beam
passes through a window into the vacuum chamber and is
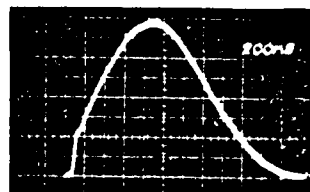focused with a 5-cm focal length lens onto the stainless-steel

substrate. The laser beam is incident on the substrate at an
angle of 30° with respect to the substrate normal, and the
spot diameter is nominally 0.1 cm. For an output energy of 1
J the irradiance at the substrate surface is approximately
2×10^8 W/cm^2 (130 J/cm^2). The beam energy is monitored
by a Gentec Joulemeter which looks at a portion of the inci-
dent beam picked off by a quartz beam splitter. The beam
temporal profile is monitored with an MRD510 PIN diode
which looks at scattered light from the vacuum chamber
window. A typical output signal from the PIN diode is
shown in Fig. 2.

The solid hydrogen slabs are fabricated by freezing liq-
uid hydrogen in a liquid helium cooled mold. The frozen
hydrogen is then extruded from the mold with a piston into
the focal region. The stainless-steel substrate is attached to
the mold so that when the hydrogen slab is extruded it is
adjacent to the substrate. The size of the solid hydrogen slab
is determined by the size of the mold. Two sizes were used in
this experiment. The slab dimensions were $0.3 \times 0.3 \times 0.025$
cm and $0.3 \times 0.3 \times 0.060$ cm. The laser spot was at the center
of these slabs.

Diagnostics used in the experiment include fast-fram-
ing and streak photography to photograph the event, a Fara-
day cup to measure ion blowoff, and a piezoelectric probe to
measure neutral particle blowoff.

The fast-framing and streak camera used in this experi-
ment is a TRW Model ID image convertor camera with an S-
11 photocathode spectral response. The camera viewed the
event from the side at an angle of 90° with respect to the
substrate normal. A lens was used to magnify the image. For
streak photographs a 0.025-cm slit positioned between the
magnifying lens and the camera provides spatial resolution.
A strobe light was used to obtain fast-framing shadow pho-
tographs. Laser light was removed by a filter in front of the
camera lens. A synchronization pulse from the laser was
used to trigger various delay generators, which, in turn, trig-
gered the image convertor camera and the strobe light. In the
framing mode the camera produces three frames with vari-
able exposure times and spacing. The frame exposure time in
this experiment is 200 ns. A frame monitor signal from the
image convertor camera was added to the PIN diode signal
and displayed on a storage oscilloscope. Accurate timing
information about the photographs is obtained in this way.

The Faraday cup probe used in this experiment has two
permanent magnets in front of it too. This provides a mag-
netic field of approximately 0.05 T which removes electrons
from the blowoff, so that the total ion current is measured.
The probe is similar to one described by Pelah.[5] The probe is
inserted through various ports in the vacuum chamber to
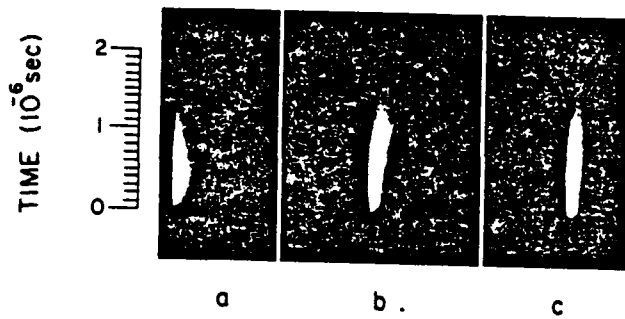measure ion blowoff at different angles with respect to the

FIG. 3. Typical streak photographs for the laser beam incident on (a) the stainless-steel substrate, (b) a 0.060-cm-thick hydrogen slab against the substrate, and (c) a 0.025-cm-thick hydrogen slab against the substrate.

substrate normal. Measurements were made with the probe at angles of 0°, 30°, and 90°.

The piezoelectric probe is similar to an arrival-time gauge described by Jones and Vlases.[6] The sensing element used here is a 1.2-cm-diam PZT-5H piezoelectric disk. The piezoelectric probe is inserted in the vacuum chamber for measurements of neutral particle blowoff at angles of 0°, 30°, and 90° with respect to the substrate normal.

All measurements were made with the vacuum chamber at a pressure of 2×10^{-4} Torr. Further details on the experimental apparatus are given in Ref. 7.

III. EXPERIMENTAL RESULTS

A. Streak photography

Figure 3(a) is a typical streak photograph, looking parallel to the target surface, for the laser beam incident on the stainless-steel substrate, with a laser energy of 2 J. Figure 3(b) is a streak photograph for a laser energy of 3 J incident on a 0.060-cm-thick hydrogen slab against the substrate, and Fig. 3(c) is a streak photograph for a laser energy of 2 J on a 0.025-cm-thick hydrogen slab against the substrate. Time and distance scales are indicated in the figure. Note that for Figs. 3(a) and 3(b) the slit was imagining the central portion of the plasma while for Fig. 3(c) the slit was imaging toward the edge of the plasma. In Figs. 3(b) and 3(c) the front surface of the luminous region exhibits a "break point" which is interpreted as the time at which the front surface of the hydrogen slab starts to move. For the 0.060- and 0.025-cm-thick slabs these times are approximately 500 and 250 ns, respectively.

B. Framing photography

Figure 4 is a collection of framing photographs taken at the indicated times for the laser beam incident on the stainless-steel substrate. Also shown is a sketch to aid in interpreting the photos. The event is luminous for only the first 10^{-6} s or so. After this time, backlighting by the strobe light provides shadow photographs. This figure is presented for the
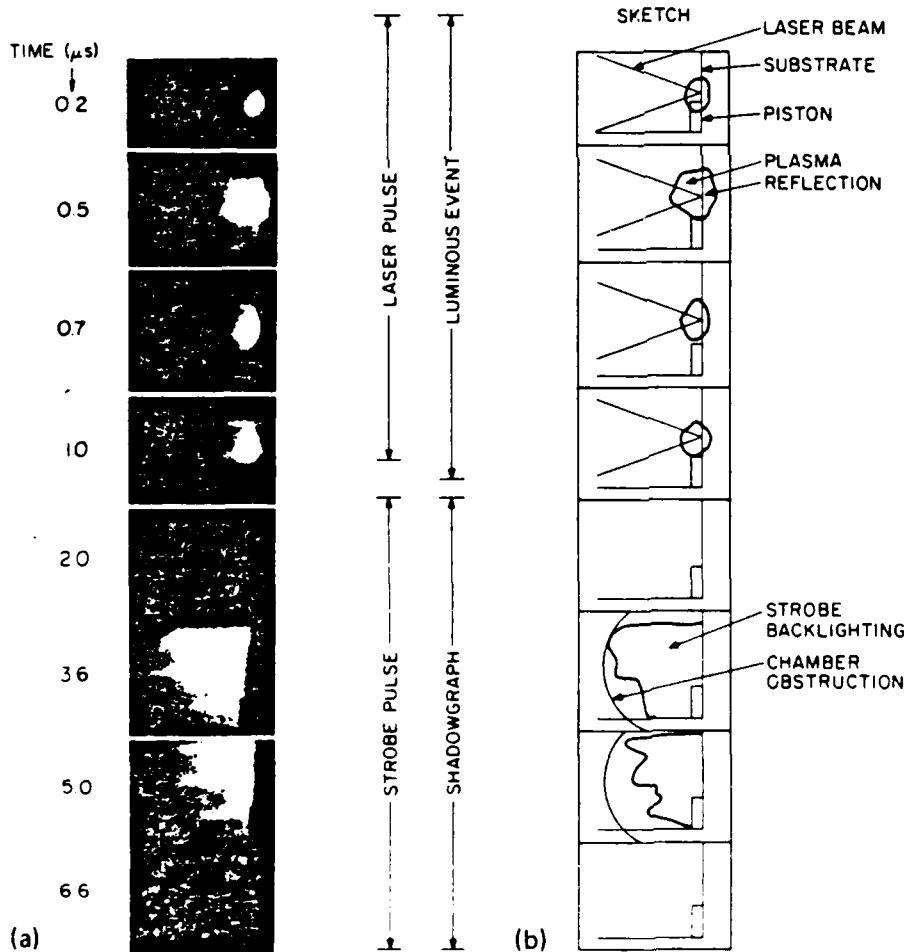

FIG. 4. (a) Framing pictures taken at various times for the laser beam incident on the stainless-steel substrate. (b) Sketches to aid in interpreting the photographs.
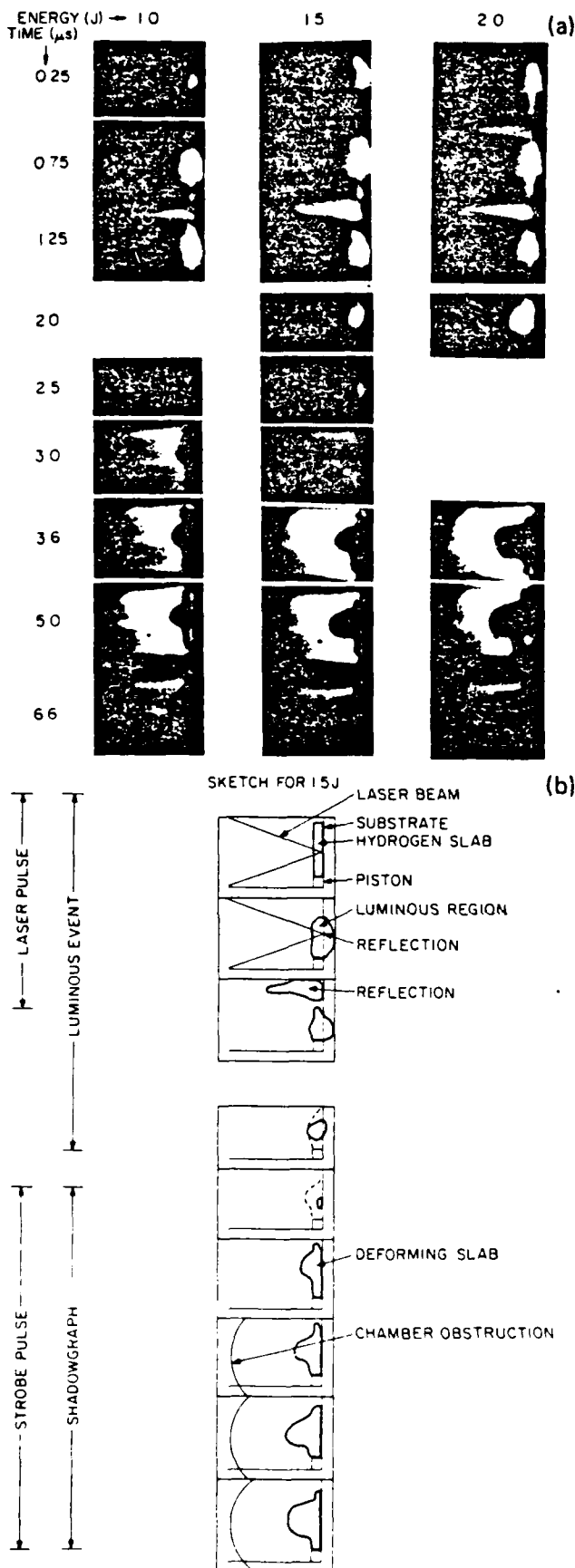
FIG. 5 (a) Framing pictures taken at various times for the laser beam incident on a 0.060-cm-thick-hydrogen slab against the stainless-steel substrate. (b) Sketches to aid in interpreting the photographs.

purpose of comparison with framing photos with the hydrogen slabs present.

Figure 5 is a collection of framing pictures at various times for various energies for the case of the laser beam incident on a 0.060-cm-thick hydrogen slab against the stainless-steel substrate. It appears from these photos that the plasma is confined behind the slab. At later times the shadow photographs show a pressure-induced deformation of the hydrogen target. The velocity of the expanding hydrogen is of the order of 10^3 m/s. From this, one can get an idea of the magnitude of the pressure generated between the substrate and the hydrogen slab. Assuming a constant pressure exerted for the duration of the laser pulse, a simple impulse calculation yields a pressure of approximately 4×10^7 Pa (400 atm).

Figure 6 is a collection of framing pictures at various times for various energies for the case of the laser beam incident on a 0.025-cm-thick hydrogen slab against the stainless-steel substrate. In these photographs one can clearly see the hydrogen plasma expanding away from the substrate. This expanding plasma is first seen in the photographs taken at $t = 0$. Since the exposure time here is 200 ns, all that can be said is that the hydrogen started expanding sometime in the first 200 ns. The velocity of propagation of the luminous boundary is of the order of 2×10^3 m/s. In this case the expansion of the hydrogen is much more violent than the expansion of the thicker target. It also appears that the luminous plasma is surrounded by the expanding cooler hydrogen.

C. Charge collection

Figure 7 shows typical oscilloscope traces of the Faraday cup probe signals with the probe at 0° with respect to the substrate normal at a distance of 7 cm. Figure 7(a) is the signal for the case of the laser beam incident on the stainless-steel substrate only. Figures 7(b) and 7(c) are the signals for the 0.060- and 0.025-cm-thick hydrogen slabs against the substrate. The initial pulse in each trace is the saturated output of the PIN diode, and is used for timing. For the 0.060-cm-thick slab, very little charge is collected. This is consistent with the framing photographs where one sees the hydrogen plasma confined between the substrate and the cold hydrogen. For the 0.025-cm-thick slab, considerable charge is collected. Note that this signal has already returned to zero at about the same time that the charge signal in Fig. 7(a) is starting to rise. The signal of Fig. 7(c) represents a charge of 4×10^{-9} C. If the ion expansion is assumed to be hemispherical, the total charge emitted from the hydrogen plasma is approximately 2.5×10^{11} ions. More will be said of this later.

Figure 8 is a summary of the charge collection measurements. The data shown are the average ion velocity versus laser beam energy for the laser beam incident on the stainless-steel substrate and for the 0.025-cm-thick hydrogen slab against the substrate. (Data for the 0.060-cm-thick slab are not shown because very little charge was measured.) The data collected fell along the various curves with a scatter which is represented by the error bars. The average velocity was calculated from the time between the peak of the pulse and the beginning of the laser pulse. (This yields a conserva-

ENERGY (J) — 1 0   1 5   2 0
TIME (µs)

~0

0.5

1.0

1.5

2.0

3.0

3.6

5.0

6.6

SKETCH FOR 2.0 J   (b)

LASER BEAM
SUBSTRATE
HYDROGEN SLAB
PISTON

LUMINOUS REGION

CHAMBER OBSTRUCTION
EXPANDING HYDROGEN

LASER PULSE
LUMINOUS EVENT
STROBE PULSE
SHADOWGRAPH

FIG. 6. (a) Framing pictures taken at various times for various energies for the laser beam incident on a 0.025-cm-thick hydrogen slab against the stainless-steel substrate. (b) Sketches to aid in interpreting the photographs.

FIG. 7. Faraday cup signals for (a) stainless-steel substrate, (b) 0.060-cm hydrogen slab, and (c) 0.025-cm hydrogen slab.

500mV   2µS.   (a)   1 0

50mV   2µS   (b)

100mV   2µS.   (c)

A) Probe At 0° Off Target Normal

B) Probe At 30° Off Target Normal

C) Probe At 90° Off Target Normal

AVERAGE VELOCITY (10⁴ m/s)

LASER ENERGY (J)

Hydrogen

Stainless Steel

FIG. 8. Average ion velocity as a function of laser energy for a 0.025-cm hydrogen slab and bare stainless steel. Maximum velocity is approximately 1.5 times the average velocity.

FIG. 9. Typical piezoelectric probe signals (a) 0.025-cm hydrogen slab, heating signal only, (b) stainless-steel substrate including effects of blow off, and (c) 0.025-cm hydrogen slab including pressure effects.

the initial heating and pressure pulses back and forth through the probe. Note that for both hydrogen slab configurations, the signal most often obtained was that of Fig. 9(a), while only occasionally were signals like that of Fig. 9(c) obtained, and then most often for the thinner hydrogen slab. Although now shown here, the probe signal contains another pressure-induced portion which occurs at approximately 2.5×10^{-5} s. This is entirely consistent with the fast-framing photographs. The thicker hydrogen slab never bursts so that only light reaches the probe, whereas the thinner target does burst. The particle velocity deduced from Fig. 9 is approximately 2×10^4 m/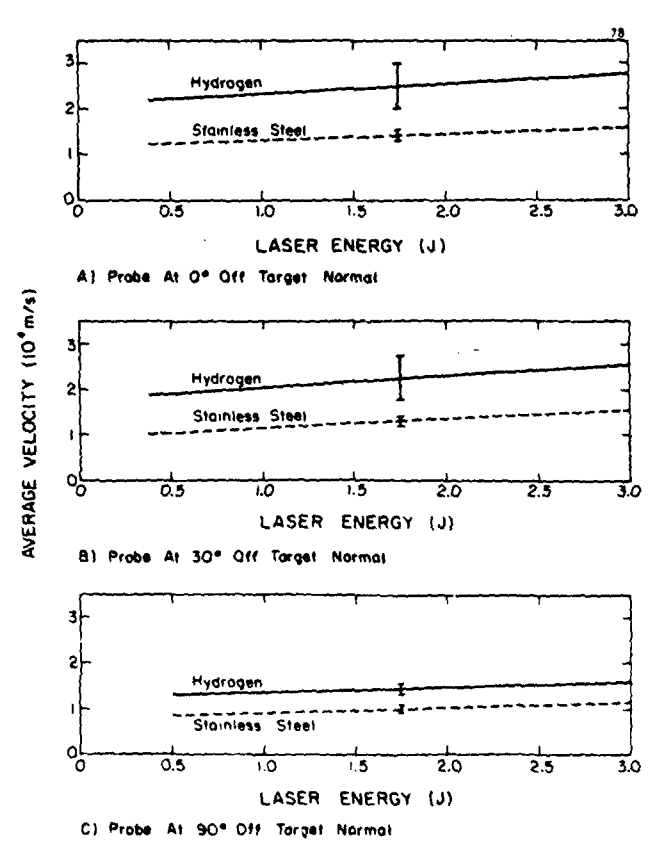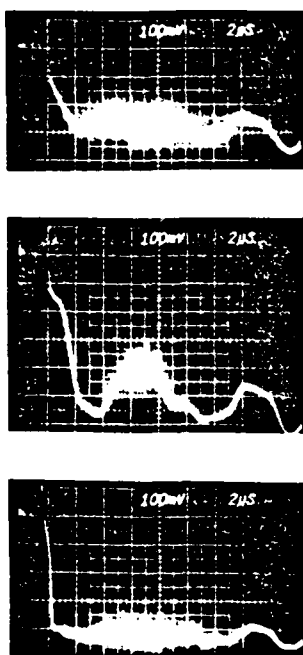s, which is an order of magnitude greater than the observed velocity of the blowoff in the framing photographs. The blowoff observed in the framing photographs causes the pressure signal at 2.5×10^{-5} s. A particle velocity of 2×10^4 m/s is consistent with the average ion velocity, but the magnitude of the probe signal is such that ions could not be responsible for causing it. The signal is due to hot neutral hydrogen which bursts through the hydrogen slab. The signal is seen only occasionally because of the way the slab bursts.

IV. MODEL FOR LASER HEATING OF SOLID HYDROGEN ON A METALLIC SUBSTRATE

A. Introduction

In order to explain the experimental results, a model for laser heating of hydrogen on a metallic substrate was developed. It involves two distinct stages (the second stage may not occur for thin targets) with different controlling phenomena. At the beginning of the laser pulse, the light energy is absorbed at the surface of the metallic substrate, initiating the first heating stage. Immediately, a hydrogen gas layer is formed by ablation between the solid hydrogen and the plasma at the metallic substrate. The light energy deposited in the plasma at the substrate surface goes into heating the gas layer. The rise in gas pressure associated with this heating drives a shock wave into the solid hydrogen which causes the shocked hydrogen to move away from the substrate surface. The heated gas expands as the hydrogen moves and natural heat convection to the solid hydrogen surface causes ablation of more hydrogen gas. Depending on the thickness of the hydrogen, at some time the shock may become strong enough to vaporize the solid hydrogen. This is the onset of the second heating stage. In the second heating stage the number of molecules in the gas is determined by propagation of the shock wave and not by ablation. During the first stage the temperature of the gas increases, but during the second state the temperature decreases rapidly due to the large influx of cold vaporized hydrogen produced by the shock wave.

tive value of the expansion velocity because of the finite time it takes for the heating disturbance to reach the front of the slab. It is actually this time that should be used for the velocity calculations. The difference, however, is perhaps 15% and for simplicity, the beginning of the laser pulse was used to determine the velocity because of uncertainty of the propagation time for different laser energies.)

Note that the velocity of the fastest ions is approximately 1.5 times the average ion velocity for both hydrogen ions and ions coming off the stainless steel. This is indicated in the caption of Fig. 8.

The maximum velocity of expansion of the ions (the velocity of the plasma front) is of considerable interest because it is possible to relate the expansion velocity to the temperature of the plasma before it expanded. Mirels and Mullen[8] derived the asymptotic flow velocity for a spherical expansion. (The derived velocity is $V_\infty = 2(\gamma RT/m)^{1/2}/\sqrt{3}(\gamma - 1)$.) Using their result, for $V_\infty = 3 \times 10^4$ m/s and $\gamma = 9/7$, the calculated temperature is approximately 10 300 K.

D. Piezoelectric probe

Typical piezoelectric probe signals for various experimental situations are shown in Fig. 9. (In this case the probe was positioned at 0° with respect to the substrate normal at a distance of 4 cm from the substrate.) The probe signals are complex, produced by a superposition of effects from pressure, heating, and mechanical oscillations. Figure 9(a) shows the heating portion of the signal, due to reflected laser light. Figure 9(b) shows the superposition of the heating signal and the signal carried by blowoff from the stainless-steel substrate, in addition to an oscillation signal. Figure 9(c) shows the superposition of the heating signal, the signal caused by blowoff from a 0.025-cm-thick hydrogen slab, and to oscillation signals. The oscillation signals are due to reflections of

We propose that during the heating process the hydrogen is subject to a Rayleigh-Taylor instability because the hydrogen gas is accelerating much more dense liquid and solid hydrogen. (The shock wave melts the hydrogen long before it begins to vaporize it.) The instability has a growth rate which depends on the acceleration of the interface. For thin hydrogen slabs the instability causes the heated hydrogen gas to burst through the free surface of the shocked hydrogen and then expand into the vacuum. For thick slabs the

instability dies due to the onset of the second stage heating process.

B. First stage heating model

The first stage of heating has the laser energy being absorbed on the surface of the metal substrate. It is then transferred to the hydrogen gas layer which exists between the metal and the solid hydrogen. This gas is heated, and the resulting high pressure drives a shock wave into the solid hydrogen. The hot gas also ablates more molecules from the solid hydrogen surface. In order to quantify these effects the following variables are defined:

$N(t)$ = the total number of hydrogen gas molecules,
$n(t)$ = the number density of hydrogen gas molecules,
$p(t)$ = the pressure of the hydrogen gas,
$T(t)$ = the temperature of the hydrogen gas,
$v(t)$ = the velocity of the shocked solid hydrogen
$V(t)$ = the volume between the substrate and the shocked solid hydrogen.

It is assumed that mixing of the gas produces uniform density and temperature. Since the laser energy goes into heating the gas and into motion of the solid hydrogen, conservation of energy gives

$$\partial/\partial t\,(Nc_v T) + pVA = qA, \tag{1}$$

where q is the intensity of absorbed laser light, A is the area of the laser spot, and c_v is the specific heat of the gas. The energy needed to ablate the hydrogen molecules is negligible compared to the internal energy of the gas.

The relationship between the pressure and the velocity of the shock wave in the solid is given by[9]

$$p = \rho_0 c_0 v, \tag{2}$$

where ρ_0 is the solid hydrogen density and c_0 is the velocity of sound in solid hydrogen. The equation of state for the hydrogen gas is

$$p = nkT. \tag{3}$$

The density n is related to the number of atoms N and the volume between the substrate and the shocked solid V by the relation

$$n = N/V. \tag{4}$$

The volume V is dependent on the velocity of shocked hydrogen $v(t)$ and the ablation rate $\partial N/\partial t$ by the relation

$$\frac{\partial V}{\partial t} = Av + \frac{m}{\rho_0}\frac{\partial N}{\partial t}, \tag{5}$$

where m is the molecular mass.

Molecules are ablated from the surface at a rate dependent on the convective heat flux to the surface Q and the heat of vaporization per molecule h_v. The relation for the ablation rate is

$$\frac{\partial N}{\partial t} = \frac{Q}{h_v}. \tag{6}$$

The convective heat flux Q is given by the Eq.[10]

$$Q = (\text{Nu})kA\,\frac{T}{x}, \tag{7}$$

where Nu is the Nusselt number, k is the thermal conductiv-

ity of hydrogen gas, and $x = V/A$ is the thickness of the gas layer.

This equation is identical to the heat flow equation for conduction through a plane wall except for the Nusselt number. The Nusselt number is a factor which takes into account the additional heat transfer due to convection. Since the shock wave travels much faster than the ablation, the second term in Eq. (5) can be neglected giving a relation between the volume V and the absorbed laser intensity q. For $\text{Nu} = 5$ (this value is consistent with the parameters in our system) and $c_v = 5/2k$, this relation is

$$V\frac{\partial^2 V}{\partial t^2} + \frac{7}{5}\left(\frac{\partial V}{\partial t}\right)^2 = \frac{2A^2}{5\rho_0 c_0}q. \tag{8}$$

The laser intensity at the beginning of the pulse can be approximated by $q = q_0 t$ W/(m²). Then, for $A = 7.85 \times 10^{-7}\,\text{m}^2$, $\rho_0 = 90\,\text{kg/m}^3$, and $c_0 = 200\,\text{m/s}$,

$$V\frac{\partial^2 V}{\partial t^2} + \frac{7}{5}\left(\frac{\partial V}{\partial t}\right)^2 = 1.37 \times 10^{-18}q_0 t. \tag{9}$$

A solution is obtained by assuming the functional form for V is $V = ct^n$. The solution is

$$V = 5.9 \times 10^{-10}q^{1/2}t^{3/2} \;(\text{m}^3), \tag{10a}$$

$$T = 5.8 \times 10^{-1}\,q_0^{3/5}t \;(\text{K}), \tag{10b}$$

$$N = 1.5 \times 10^{16}\,q_0^{2/5}t \;(\text{particles}), \tag{10c}$$

$$n = 2.5 \times 10^{25}\,q_0^{-1/10}t^{-1/2} \;(\text{m}^{-3}), \tag{10d}$$

$$p = 2.0 \times 10^2\,q_0^{1/2} \;(\text{Pa}), \tag{10e}$$

and

$$v = 1.1 \times 10^{-3}\,q_0^{1/2}\,t^{1/2} \;(\text{m/s}). \tag{10f}$$

The first stage heating model is no longer valid at the time when the shock wave traveling into the solid hydrogen is strong enough to vaporize the hydrogen, because then the ablation into the gas volume is primarily due to the shock and not the gas heating. The following equations allow that time to be determined. The internal energy of the shocked solid hydrogen is

$$E = \frac{p^2 c}{2\rho_0}, \tag{11}$$

where C is the compressibility of solid hydrogen. Using $C = 4 \times 10^{-9}\,\text{m}^2/\text{N}$[11] and Eq. (10e) for the pressure one obtains

$$E = 8.9 \times 10^{-7}\,q_0 t. \tag{12}$$

The heat of vaporization for solid hydrogen is 4.6×10^5 J/kg. Then the time for shock-induced vaporization τ_{sv} is

$$\tau_{sv} = 5.2 \times 10^{11}q_0. \tag{13}$$

The laser light intensity in this experiment increases approximately as $10^{19}t$ W/m². However, the intensity of the absorbed laser light will be less than this due to reflections at the substrate surface and heat absorption by the substrate. Therefore, a more realistic absorbed intensity is of the order of $10^{18}t$ W/m². The temperature T is plotted versus time in Fig. 10 for q_0 values of 10^{18}, 3×10^{18}, and 10^{19}. The temperature increases until the time τ_{sv}, at which time the second stage heating model begins.
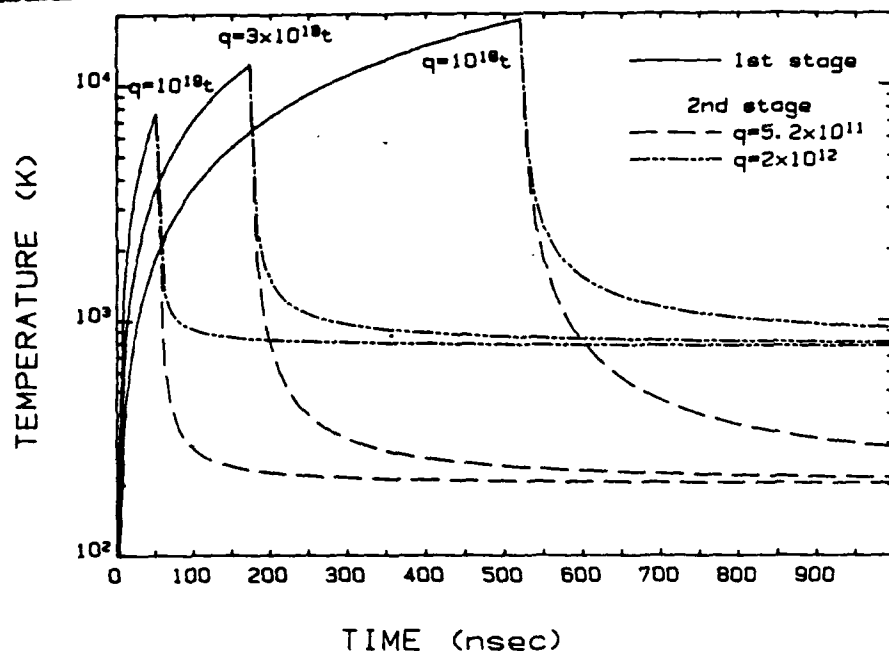
FIG. 10. Theoretical plot of temperature as a function of time for various laser energies. In the first stage the laser energies vary linearly with time. In the second stage the energies are constant. All energies are in W/m^2. The sharp declines are where the second stage heating starts.

C. Second stage heating model

The second stage heating model comes into play when the shock wave in the solid is strong enough to vaporize the solid. Equations (1–4) of the first stage heating model are still valid in the second stage model. However, the rates of change of the volume of hydrogen gas and the number of molecules are now dependent on the velocity of the shock. (The number of gas molecules is now increasing dramatically.) We have

$$\partial V / \partial t = c_0 A \qquad (14)$$

and

$$\partial N / \partial t = n_s c_0 A, \qquad (15)$$

where n_s is the density of solid hydrogen. Equations (14) and (15) can be solved to obtain

$$V = c_0 A t + V_0 \qquad (16)$$

and

$$N = n_s c_0 A t + N_0, \qquad (17)$$

where $V_0 = V(\tau_{sv})$ and $N_0 = N(\tau_{sv})$ are the initial conditions obtained from the first stage model.

Combining Eqs. (1–4), (16), and (17) yields the following first-order differential equation for the temperature:

$$\frac{dT}{dt} + \left(\frac{1}{t+a} + \frac{2/5}{t+b}\right) T = \frac{c}{t+a}, \qquad (18)$$

where

$$a = N_0 / n_s c_0 A,$$

$$b = V_0 / c_0 A,$$

and

$$c = q / n_s c_0 c_v.$$

A solution for T can be obtained by assuming $q = $ constant. Then

$$T = \left(T_0 - \frac{5}{7} \frac{bc}{a}\right)\left(1 + \frac{t}{a}\right)^{-1}\left(1 + \frac{t}{b}\right)^{-2/5}$$

$$+ \frac{5}{7} \frac{bc}{a}\left(1 + \frac{t}{a}\right)^{-1}\left(1 + \frac{t}{b}\right), \qquad (19)$$

where $T_0 = T(\tau_{sv})$ from the first stage model.

The laser intensity at $t = \tau_{sv}$ from the first stage model is $q = 5.2 \times 10^{11}$ W/m^2. The peak laser intensity for 1-J output is 2×10^{12} W/m^2. The solution to Eq. (19) for $q_0 = 5.2 \times 10^{11}$ and $q_0 = 2 \times 10^{12}$ is shown in Fig. 10 for the various first stage model conditions. This range of intensities includes the experimental values. From this one can see that even if 100% of the incident laser light were absorbed, the temperature drops very rapidly. Hence, if the shock-induced vaporization time is reached, the desired temperature range of 3000–6000 K cannot be attained. The actual temperature is not of interest for that reason. For successful operation the parameters of the system must be such that the second stage is not reached.

D. Rayleigh-Taylor instability

The hot hydrogen gas is accelerating the solid hydrogen. If the solid is liquefied or if the forces on the solid are high enough that it can essentially flow like a liquid, then the conditions for a Rayleigh-Taylor instability are present. After a very short time in the heating process the energy given to the shocked hydrogen is greater than the heat of fusion; thus the shocked hydrogen is liquefied. Now we have a hot gas beneath a liquid beneath the solid unshocked hydrogen. We propose a Rayleigh-Taylor instability which is free to grow into the liquid. This instability grows with a characteristic time

$$\tau_{RT} = \left(\frac{\lambda}{a}\right)^{1/2},$$

where λ is the wavelength of the instability and a is the acceleration of the interface, obtained by differentiating Eq. (10f).

Instabilities with wavelengths of the order of the target thickness grow with characteristic times which are comparable to the shock-induced vaporization time.

So for thin slabs it is likely that the Rayleigh-Taylor instability will occur and the hot gas will burst through the hydrogen before the onset of the second stage heating. For thicker slabs, where the instability growth time is greater than the shock-induced vaporization time, the instability dies. At this time, however, the vaporization front is moving at the sonic velocity, which is faster than the instability growth, so in a sense the instability is overcome. If the slab is thin enough, the Rayleigh-Taylor instability gives a mechanism which will allow the desired temperatures.

V. COMPARISON OF THE HEATING MODEL WITH THE EXPERIMENTAL RESULTS

In the comparison of the experimental results with the model, it is not possible to get exact values for all quantities, and for that reason precise correlations could not be done. In the following comparison the absorbed laser intensity during the first heating stage is assumed to be $2 \times 10^{18} t$ W/m^2, which corresponds to 20% absorption. With this assumption for the 0.025-cm-thick hydrogen slab, the shock reaches the free surface of the hydrogen in 125 ns, and the instability growth time for $\lambda = 0.025$ cm is about 100–200 ns. The time for instability is short compared to the time needed for the shock wave to become strong enough to produce vaporization. From the fast-framing photographs one can see a luminous plume of material flowing from the hydrogen slab within the first 200 ns. From the heating model the temperature of the gas at $t = 200$ ns is approximately 10 000 K. We conclude both from the model and from the experiment that the hot gas bursts through the hydrogen and expands into the vacuum. Using Eq. (10c), the number of molecules in the gas at this time is calculated to be approximately 8×10^{16}. The fractional ionization from the Saha equation for hydrogen at $T = 10\,000$ K is approximately 1×10^{-3}. Then the number of ions in the gas is approximately 8×10^{13}, which is in reasonable agreement with the value 2.5×10^{13} ions deduced from the Faraday cup signals. Also, the temperature is in agreement with the experimentally deduced temperature of $T = 10\,300$ K from the ion time of flight. Also, due to the turbulent nature of the expansion, as seen in the fast-framing photographs, the infrequent detection of fast neutrals by the piezoelectric probe is reasonable. The expansion velocity of colder hydrogen as seen in the fast-framing photographs and as detected by the piezoelectric probe is of the order of 2×10^3 m/s. This is consistent with the heating model where the velocity of shocked hydrogen is of the order of 1×10^3 m/

s and the velocity doubling effect which occurs at the free surface of the hydrogen when the shock reaches it.[9]

Experimental results for the 0.060-cm-thick hydrogen slab contrast sharply with those for the 0.025-cm-thick slab. From the framing pictures one sees that the hydrogen gas doesn't burst through the first surface of the slab. The hydrogen is simply deformed into a hemispherical shape by the pressure of the gas. The time for the shock wave to propagate through the slab is 300 ns while the shock-induced vaporization time is 260 ns. Thus, the second stage heating process begins, and the Rayleigh-Taylor instability does not occur. At $t = 300$ ns the hydrogen is completely vaporized, and the temperature from the second stage model is approximately 600 K. The fractional ionization at this temperature is very small which is consistent with the Faraday cup signals which are small. The pressure calculated from the equation of state during the first and second stages of heating is in the range 10^7–10^8 Pa, which agrees with the average pressure of 4×10^7 Pa deduced from the velocities seen in the fast-framing photographs.

In conclusion, the heating model presented here explains to a reasonable degree of accuracy the experimental observations for both hydrogen slab thicknesses. In view of the above, hydrogen gas temperatures in the range 3000–6000 K can be obtained by suitable choice of laser intensity and hydrogen slab thickness. The slabs would have to be thin enough to prevent the second heating stage from occurring. Also, although it was not treated here, the target must be thin so that the amount of mass expanding into vacuum is small enough to prevent vibrational deexcitation. Thus the conditions for nonequilibrium production of vibrationally excited hydrogen molecules could be attained using this laser heating technique.

[1]M. M. Menon, Proc. IEEE 69, 1012 (1981).
[2]M. Bacal, A. M. Brunetau, W. G. Graham, G. W. Hamilton, and M. Nachman, J. Appl. Phys. 52, 1247 (1981).
[3]S. R. Walther, M.S. thesis, Electrical Engineering Department, University of Illinois, 1984.
[4]K. N. C. Bray, in *Nonequilibrium Flows*, edited by P. P. Wegener (Dekker, New York, 1970), Part II, p. 59.
[5]I. Pelah, Phys. Lett. A 59, 348 (1976).
[6]T. G. Jones and G. C. Vlases, Rev. Sci. Instrum. 38, 1038 (1967).
[7]J. L. Guttman, Ph.D. thesis, Department of Electrical Engineering, University of Illinois, 1982.
[8]H. Mirels and J. F. Mullen, AIAA J. 1, 596 (1963).
[9]Y. B. Zel'dovich and Y. P. Raizer, *Physics of Shock Waves and High Temperature Hydrodynamic Phenomena* (Academic, New York, 1967), Vol. II, p. 742.
[10]J. R. Welty, *Engineering Heat Transfer* (Wiley, New York, 1974), p. 11.
[11]H. M. Roder, G. E. Childs, R. D. McCarty, and P. E. Angerhofer, *Survey of the Properties of the Hydrogen Isotopes Below Their Critical Temperatures* (U.S. Department of Commerce, Washington, D.C., 1973), p. 28.

III. Fabrication of planar and cylindrical solid hydrogen pellets for laser interaction experiments

J. L. Guttman[a] and R. J. Turnbull

Department of Electrical Engineering, University of Illinois, Urbana, Illinois 61801

A system is described for fabricating both planar and cylindrical solid hydrogen pellets. The target geometry is determined by the geometry of interchangeable target molds. Planar targets fabricated with this system have dimensions of 3.0×3.0 mm with thicknesses ranging from 0.13 to 0.60 mm, and cylindrical targets were 1.0–3.0 mm in length with diameter of 0.80 mm.

INTRODUCTION

A number of hydrogen pellet fabrication systems have been described in the literature. Francis et al.[1] used a system in which deuterium gas precooled to 25 K is frozen inside a cylinder cooled with liquid helium to 5 K. A piston then forces the frozen deuterium into a channel from which pellets are "punched out" by a second piston. The pellets produced were 0.25 mm in diameter and 0.25 mm in length and were ejected with a velocity of 10^3 cm/s. These pellets were then ejected so that they fell to the focal region of a laser beam. The authors expressed doubts about the homogeneity of the pellets they produced. (Homogeneity means here that the ice is uniform and clear, as opposed to slushy or granular.)

Cecchini et al.[2] condensed deuterium inside a liquid-um-cooled capillary tube and formed a pellet by compressing the condensate between a piston and a plug. After compression, the plug was removed and the pellet ejected by application of a heat pulse using either a rf source or a heat lamp. Pellet diameter was determined by the distance between the piston and the plug which was adjustable down to a length of 0.2 mm.

Bobin et al.[3] used a solid deuterium pellet obtained from condensing gas inside a liquid-helium-cooled extruder. The targets were a few millimeters long with square cross section 1 or 2 mm on a side. The pellets were extruded with a piston into the focal region.

Sigel et al.[4] produced planar solid hydrogen pellets by condensing gaseous hydrogen into a hole in a liquid-helium-cooled copper block. Careful regulation of the temperature of the block enabled them to produce homogeneous hydrogen ice. The diameter was 2 mm and the thickness, which varied as to how much gas was condensed, was initially about 1 mm, but diminished as a function of time due to slow vaporization. In this case, the focal region is the hole where the pellet is formed. Also, a modification of the system was used to produce cylindrical pellets 0.1 mm in diameter and 0.1 mm in length using a piston arrangement.

Foster et al.[5] formed solid hydrogen spheres by breaking up a liquid jet and then freezing the resulting drops. The liquid was formed using heat exchangers and instrumentation similar to that of this paper.

With the solid hydrogen pellet fabrication system described here, the pellet is formed by flowing liquid hydrogen into a liquid-helium-cooled mold where the liquid hydrogen freezes. The frozen hydrogen pellet is then extruded from the mold and positioned in the focal region using a piston. The size and shape of the pellet are determined by the mold, which is interchangeable. Both planar and cylindrical pellets have been fabricated. The planar targets are 3 mm wide with thickness ranging from 0.13 to 0.60 mm, and the cylindrical targets are 0.8 mm in diameter. The length of the target is determined by the piston position in the mold and is usually 3 mm. Because the pellet is formed from liquid hydrogen, the ice is homogeneous. This system was designed for use in ablative pellet acceleration and laser heating experiments. The unique feature of this system is its ability to produce free standing planar pellets.

I. HYDROGEN TARGET FABRICATION SYSTEM

A block diagram of the hydrogen target fabrication system is shown in Fig. 1. The diagram shows the following main subsystems: (1) A liquid-helium-cooled heat exchanger for production of liquid hydrogen, called the hydrogen li-
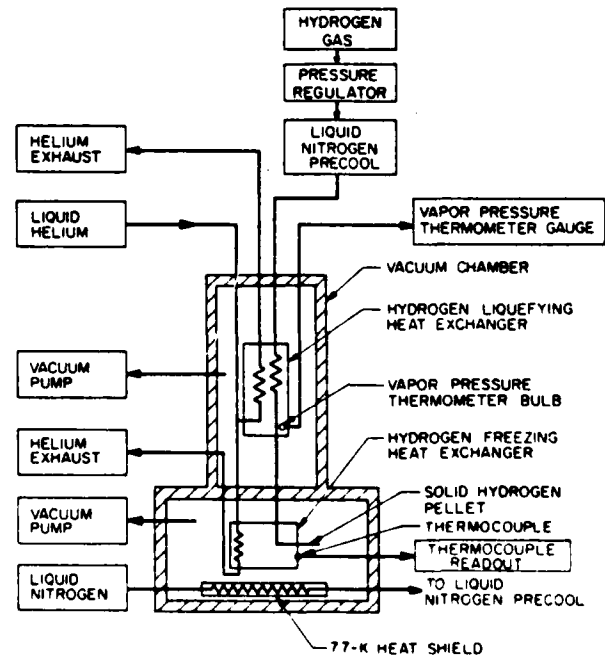

FIG. 1. Block diagram of the hydrogen pellet fabrication system.

quefying heat exchanger, (2) an interchangeable liquid-helium-cooled mold where the liquid hydrogen freezes, called the hydrogen freezing heat exchanger, (3) a liquid-nitrogen heat shield, (4) temperature measurement system, and (5) gas flow and vacuum system.

The system operates as follows: Liquid helium cools the hydrogen liquefying heat exchanger to approximately 15 K and hydrogen gas at 400 Torr is liquefied. The liquid hydrogen in turn cools the hydrogen freezing heat exchanger. When the gas pressure is reduced the liquid hydrogen flows more slowly so that additional cooling by liquid helium freezes the hydrogen. The frozen pellet is then extruded with a piston. Some particulars of the system are given below.

A. The hydrogen liquefying heat exchangers

The hydrogen liquefying heat exchanger, shown in Fig. 2, is of the counterflow coaxial type. The heat exchanger is made of OFHC copper and filled with sintered OFHC copper balls to increase the thermal conduction. Liquid hydro-

gen flows from the heat exchanger to the hydrogen freezing heat exchanger via a small diameter copper tube.

B. The hydrogen freezing heat exchanger

The hydrogen freezing heat exchanger is shown in the top view in Fig. 2. It consists of the interchangeable pellet mold and a U-shaped copper channel which hugs the sides of the mold and through which liquid helium flows. A good thermal conduction path to the mold is provided by filling the gap between the channel and the mold with Wood's metal, thus making it a solid assembly. The assembly is connected to two translational feedthroughs oriented 90° to one another, allowing positioning of the mold while the system is cold. This is necessary because the system contracts appreciably when cooled.

Figure 3 is a side view cross section of the interchangeable pellet mold. The piston enters the mold from the bottom through a gasket which forces the liquid hydrogen to flow upward into the mold region. When the hydrogen freezes in
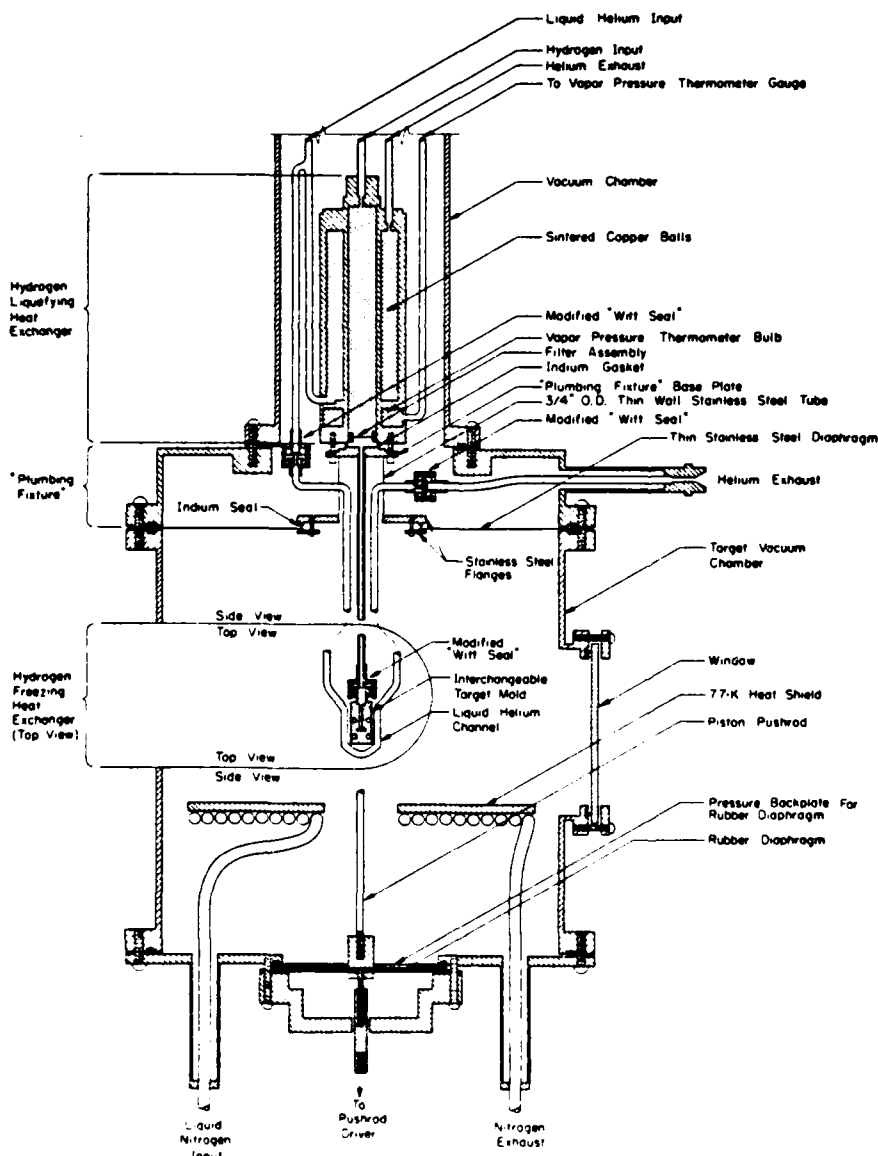

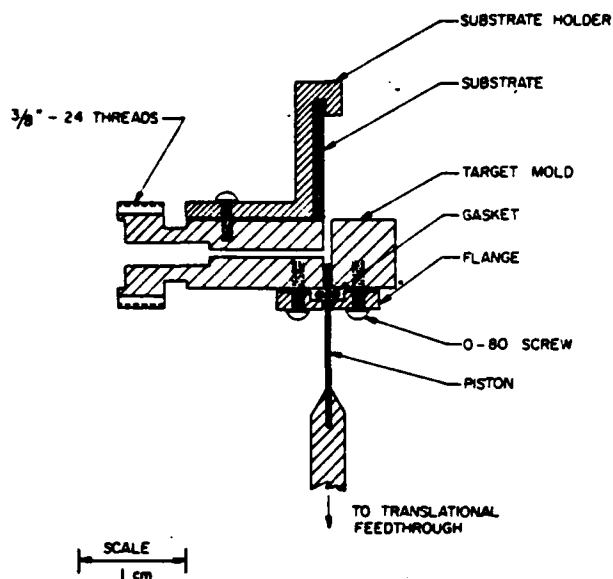FIG. 2. Cross section of the hydrogen pellet machine.

FIG. 3. Side view cross section of the interchangeable target mold, piston seal, substrate, and substrate holder.

FIG. 4. 0.25-mm-thick planar hydrogen pellet.

the mold it is extruded by extending the piston. Also shown in Fig. 3 is an optional substrate and substrate holder. The substrate was used for indirect laser heating experiments in which the laser energy was absorbed at the substrate and ·sferred to the hydrogen pellet. Ablative acceleration ex-.ments were done without the substrate.

For cylindrical pellets the mold is simply a hole drilled through the copper. For planar pellets the mold is assembled from two pieces, one of which has a milled slot in it which determines the pellet size. Lower limits on pellet diameter or thickness are determined by the ability to make a suitable piston. Ordinarily the piston material is stainless-steel wire or sheet. For very thin (0.15 mm) pellets a tungsten piston was used.

C. The liquid-nitrogen heat shield

The liquid-nitrogen heat shield is shown in Fig. 2. It consists essentially of a brass disk to which a coil of copper tubing has been soldered. Liquid nitrogen is forced through the copper tube which in turn cools the disk. When the liquid hydrogen is flowing through the hydrogen freezing heat exchanger, the pressure in the target chamber is in the order of 75 Torr. With this much pressure there is a significant convective heat flow between the hydrogen freezing heat exchanger and the target chamber wall, which is at approximately 300 K. Unless the heat shield is used, this heat flow is sufficient to prevent freezing of the liquid hydrogen in the mold.

D. Temperature measurement system

The temperature of the hydrogen liquefying heat exchanger is monitored with a hydrogen vapor pressure thermometer. The temperature of the hydrogen freezing heat exchanger is monitored with a copper-constantan thermocouple.
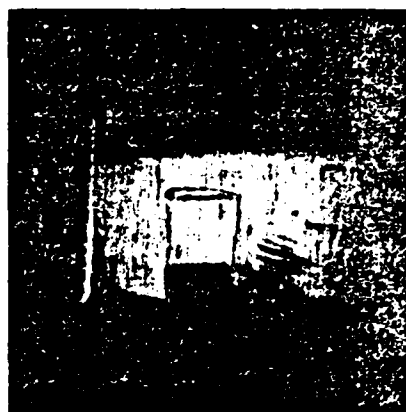
E. Gas flow and vacuum system

Hydrogen, supplied as a gas from a pressurized cylinder, flows to a Conoflow model H21AT differential pressure regulator. Upstream pressure is monitored with a Marsh Scientific Company 0–5000-Torr pressure gauge. The regulator regulates the downstream pressure in the range 0 to 800 Torr and this pressure is monitored with a Magnehelic pressure gauge, which is referenced to vacuum in order to read absolute pressure. The hydrogen then flows to the hydrogen input line of the hydrogen liquefying heat exchanger and to the vapor pressure thermometer. The vapor pressure thermometer gauge is a Magnehelic gauge with a range of 0 to 160 Torr which is also referenced to vacuum. The target chamber is connected to a Welch model 1397 mechanical vacuum pump which has a pumping speed of 500 l/min.

FIG. 5. 0.8-mm-diam cylindrical hydrogen pellet.

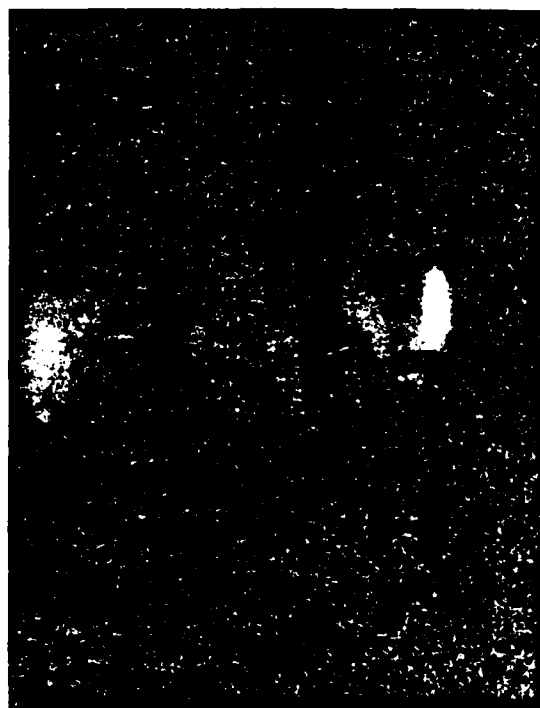This pumping speed is sufficient to maintain the target chamber pressure below 100 Torr when liquid hydrogen is flowing into the target chamber. The target chamber pressure is monitored with a vacuum reference Magnehelic gauge with a range of 0 to 100 Torr. When the pellet is frozen in the mold, the system cryopumps to approximately 10^{-4} Torr.

The liquid-helium flow schematic was shown previously in Fig. 1, the block diagram of the hydrogen pellet fabrication system. The block labeled "liquid helium" consists of a liquid-helium Dewar which is pressurized with helium gas from a gas cylinder. The liquid helium then flows through a transfer tube into the vacuum chamber. The helium flow then branches into two flow paths. One path goes to the hydrogen liquefying heat exchanger and the other goes through the vacuum chamber wall to the hydrogen freezing heat exchanger and then back through the vacuum wall again. Both lines then exit the vacuum chamber via vacuum extension feedthroughs. (One of these feedthroughs labeled "helium exhaust" is shown in detail in Fig. 3. The purpose of these feedthroughs is to prevent the entire system from getting cold by isolating the cold exit point from the vacuum chamber which is at room temperature.) The helium lines then flow to the blocks labeled "helium exhaust" which are Hoke model 7127 ball valves designed for use with liquid nitrogen. The flow rates are manually controlled by adjustment of these valves, and the exhaust flows into the atmosphere. Typical hydrogen pellets fabricated with this system are shown in Figs. 4 and 5. Figure 4 shows a 0.250-mm-thick planar pellet and Fig. 5 shows a 0.800-mm-diam cylindrical pellet.

[a] Current address: Lockheed Palo Alto Research, Palo Alto, CA 94304.

[1] G. Francis, D. W. Atkinson, P. Avivi, J. F. Bradley, C. D. King, W. Miller, P. A. H. Saunders, and A. F. Taylor, Phys. Lett. A 6, 486 (1967).

[2] A. Cecchini, A. DeAngelis, R. Gratton, and F. Parlange, J. Phys. E 1, 1040 (1968).

[3] J. L. Bobin, F. Delobeau, G. DeGiovanni, C. Fauquignon, and F. Floux, Nucl. Fusion 9, 115 (1969).

[4] R. Sigel, H. Krause, and S. Witkowski, J. Phys. E 2, 187 (1969).

[5] C. A. Foster, K. Kim, R. J. Turnbull, and C. D. Hendricks, Rev. Sci. Instrum. 48, 625 (1977).

IV.   Production of Vibrationally Excited H$_2$ in a gas Discharge
       for use in an H$^-$ Source

1. INTRODUCTION

High energy neutral beams of hydrogen isotopes are useful for heating

fusion plasmas and for other applications. The only efficient way of

generating such high energy (>150kev) beams is by accelerating negative ions

and then stripping the excess electrons to form a neutral beam. Three methods

for producing negative hydrogen ions have been used. These are volume

production in a discharge, surface production using charge exchange, and

volume production using charge exchange. Papers on each technique as well as

an overview of the status of the field can be found in Reference 1. The first

method (volume production in a discharge) is the method of interest in this

paper.

The primary reaction producing negative hydrogen ions in a gas discharge

is the dissociative attachment reaction, that is

$$H_2 + e \rightarrow H^-. \tag{1}$$

The cross section for this reaction is enhanced by orders of magnitude when

the hydrogen molecules are vibrationally excited [2], [3]. Since this cross

section is a strong function of the initial vibrational state, production of

negative ions should increase dramatically if excitation of the hydrogen

molecules is increased. To make use of this effect one can improve negative

ion generation by using two distinct discharges. The first discharge is

optimized to produce vibrationally excited hydrogen, which flows into a second

discharge where volume production of negative hydrogen ions takes place. In

this paper, work on a source of vibrationally excited hydrogen is described. The present experiment begins with a flow of high pressure hydrogen into an arc discharge. The arc discharge heats the hydrogen molecules which exit the discharge through a converging nozzle. Outside the nozzle the flow expands into an evacuated region, thus retaining most of the initial vibrational energy. A second discharge can then be located to use this flow of excited molecules to produce negative ions.

Before detailing the experiment to produce vibrational excitation, optimum conditions for creating and retaining vibrational excitation are derived, finally the experimental results are discussed.

2. THEORETICAL CALCULATIONS

In order to determine how much the negative hydrogen ion production rate can be enhanced by using a gas which has been heated and then expanded, it is necessary to calculate the amount of vibrational excitation remaining after the gas has expanded. Therefore calculations were done on the effect of the expansion on the populations of the various vibrational levels. The starting point for the calculations was at the nozzle exit where the gas was assumed to be in thermal equilibrium. The population of each vibrational level at this point was determined from equilibrium equations because of the large density present there. The gas then was allowed to expand into vacuum starting at Mach 1 at the nozzle exit. Since the heating occurs before this point, the flow was assumed to be adiabatic. The atomic and ionic fraction was assumed to be negligible.

Near the nozzle there is interaction between vibrational and

translational energies and far from the nozzle there is complete isolation
between vibrational and translational energies. Thus at some point in the
flow, the vibrational energy can be said to be frozen in. Because of the
anharmonic nature of the vibrational levels, the higher levels interact much
more strongly with the translational energy than the lower levels. As the gas
expands, collisions between molecules can result in a transfer of energy
between vibrational and translational forms. Since the gas cools rapidly the
predominant energy transfer is from vibrational to translational. Also
collisions can result in the transfer of vibrational energy between molecules.
Since the energy spacings between the vibrational levels decreases as the
level increases, this results in increasing the population of the higher
levels with some increase in kinetic energy. Therefore no analytical model
could be used to calculate the resulting populations in the expanded gas. The
calculations were done using a simple iterative technique assuming adiabatic
conditions and taking into account the vibrational-translational and
vibrational-vibrational interactions for each vibrational level. Almost all
of the interactions take place very near the nozzle throat, so after the gas
has expanded to a few nozzle radii the vibrational populations no longer
change. For a given initial temperature, the vibrational populations in the
expanded gas depend only on the product of the molecular density at the nozzle
exit and the nozzle radius. Some typical results are shown in Figures 1 and
2. Figure 1 has an intial temperature of 3000K and Figure 2 has 5000K.
Comparing the vibrational populations of the expanded gas with the initial
equilibrium values it can be seen that the higher states depopulate much
faster than the lower states. Thus the transfer of vibrational energy from
lower states to higher states is much less important than the vibrational to

translational energy transfer. Also it can be seen that a density radius product of $10^{17}cm^{-2}$ results in only the highest levels depopulating while greater initial densities result in a decreased vibrational population until an nr product of $10^{20}cm^{-2}$, which produces almost complete depopulation of the vibrational states.

Calculations were also done of the negative ion production rate from dissociative attachment (the predominant production mechanism) with the vibrational populations resulting from the expansion of the heated gas. The production was in a gas discharge with the ratio of electric field to gas density set at 40 Townsends. These are approximately the optimum conditions, but the peak is very broad. The electron distribution was calculated using a modified upflux model [4]. The rate calculated is the number of ions produced per second per molecule with a fractional ionization of .001. The results are shown in Figure 3. The results are given for a variety of initial temperatures and density radius products. The results for 5000K are overstated because of the high dissociation rate which was not taken into account. The results for nr = 10^{20} are approximately those of hydrogen in the ground vibrational state. It can be seen that it might be possible to increase the production rate by as much as two orders of magnitude using this technique.

3. EXPERIMENTAL APPARATUS AND RESULTS

3.1 Experimental Apparatus

To achieve vibrational excitation, the experimental apparatus first heats the hydrogen molecules and then expands the flow into a vacuum region through

a nozzle. This is done on a pulsed basis for two reasons. The first reason being that the energy source for discharge heating is a capacitor. Thus the discharge ends when the capacitor's energy is depleted. The second reason being that a sufficient vacuum cannot be maintained with a continuous flow of hydrogen into the vacuum system. Therefore, hydrogen must be introduced to the apparatus on a pulsed basis.

The choice exists of heating the hydrogen either before or after the nozzle. Heating after the nozzle, during the expansion of the gas, results in a choked flow. The choked flow does not expand as rapidly as an unchoked flow and, consequently, vibrational deexcitation is more likely. Fabrication of the electrodes for this method is more difficult because of the need for uniform heating. Heating of the hydrogen molecules before the nozzle was chosen to avoid these problems.

The electrodes, arc chamber, and gas valve are shown to scale in Figure 4. The gas valve is bolted to the brass flange plate and serves to introduce hydrogen into the apparatus. When operated, the valve quickly opens and lets a pressure wave of hydrogen move into the arc chamber. The arc chamber and electrodes operate inside a vacuum chamber and are mounted to the underside of the brass flange plate. When the gas valve is opened, gas moves through a hole in the flange plate into the arc chamber. The arc discharge is initiated after the gas reaches the electrodes at the bottom of the chamber. The flow of hydrogen gas is heated by the discharge and then exits the arc chamber through the nozzle. After exiting the nozzle, the hydrogen expands and cools rapidly allowing most of the vibrational energy to be retained.

Operation of the experimental apparatus was straightforward. The gas valve was actuate' by discharging four 135 μf capacitors connected in parallel

and charged to 1000 volts into the solenoid of the gas valve. An EC-431L SCR was connected in series with the solenoid and operated as a switch for the capacitor bank. The resulting pulse of gas was detected by a pressure sensing piezoelectric crystal mounted in the arc chamber close to the nozzle. The output voltage of the crystal triggered a variable delay generator which triggered an SCR. The arc electrodes are connected to a capacitor through the SCR, which acted as a switch. Arc current was monitored with a Pearson current transformer and arc voltage and capacitance could be varied as desired.

Two parameters of the arc discharge determine the vibrational excitation of the gas; these are the gas density and the gas temperature. Gas density controls dissociation as well as the rate of collisional energy transfer. Gas temperature also controls dissociation as well as vibrational excitation. Measurement of these quantities gives information about how much vibrational energy is generated in the arc and retained during the expansion of the gas flow. The next sections deal with measurements of these quantities.

3.2 Pressure Measurement

Since gas density in the arc is related to the inlet pressure used on the gas valve, a measure of the gas density in the arc discharge is needed to determine what inlet pressure to use on the gas valve. The pressure sensor used must be extremely fast acting as well as small and unobtrusive to the gas flow. Those requirements are met by using a piezoelectric crystal which produces a voltage proportional to the pressure differential applied to its faces. A thin slice of a hollow cylinder of piezoelectric crystal, mounted as a small section of the arc chamber, was used to measure the pressure and

trigger a delay generator for the arc. This piece, shaped like a doughnut, had an inside diameter slightly smaller than that of the glass chamber, which results in an unobstructed flow.

The piezoelectric crystal measured the difference in pressure between the outside and inside of the arc chamber. Since the outside of the arc chamber is always in a vacuum, the measurements correspond to absolute pressure inside the arc chamber. The gas pressure as a function of time was measured without running the arc discharge because the noise generated by the arc completely masks the signal produced by the piezoelectric crystal. Thus pressure was measured for the cool gas and a density calculated from that.

The density for the heated gas can be approximated using the ideal gas law. Assuming a uniform pressure inside the arc chamber and noting that the discharge region is small, the gas in the arc chamber can be characterized by defining an arc region with temperature T_a and a background region of temperature T_b. With a constant pressure over both regions, the density and temperatures of both regions can be related by

$$n_a T_a = n_b T_b, \qquad\qquad (2)$$

where n_a is the atomic density in the arc region, and

n_b is the atomic density in the background region. Hence, having measured the density of the cool background gas at room temperature, the density of the heated gas in the arc can be calculated when the arc temperature is known. Figure 5 shows the relationship between valve inlet

pressure, gas temperature, and gas density in the arc. Hence any desired density, until the pressure limits of the gas valve are reached, can be achieved by using the right valve inlet pressure, keeping in mind the temperature effects of the arc. The next section examines methods and experiments used to measure the gas temperature in the arc discharge.

3.3 Temperature Measurement

Of the two parameters of the arc discharge, gas density and temperature, only gas density can be easily determined. Measuring the gas temperature of hydrogen in a pulsed system is done by indirect means. Ordinarily, one can use radiation from vibrational-rotational bands to determine gas temperature. Hydrogen, though, has no electric dipole moment. This means that those bands radiate principally by electric quadrupole transitions which are extremely weak. Likewise, electronic transitions reflect electron temperature which is quite different from the gas temperature in a pulsed arc discharge. However, temperature can be determined from the velocity of the flow downstream from the nozzle. The velocity can be measured by doing time-of-flight studies on the atoms, molecules, or ions. This simply means a detection system is a known distance downstream from the nozzle and the time elapsed between discharge initiation and first detection of gas particles is the time of flight.

A second discharge downstream from the nozzle was chosen as the detection mechanism. The second discharge is run as an ionization gauge would be. The filament is electrically heated and emits electrons which are attracted to the potential on the anode. The discharge current is dependent upon the density of the gas present through electron impact ionization of the gas. Therefore,

this method can monitor pressure fluctuations with time and detect the leading edge of the gas pulse from the arc discharge.

Operation of the second discharge is controlled by the filament current and the anode to filament voltage. The filament was taken from an ionization gauge tube, so operating conditions of the tube were used for the second discharge. An easily measured discharge current was present even at pressures of 10^{-6} torr. The initial pulse of electrons created by the arc was also detected much earlier than the pulse due to the gas flow. Typical oscilloscope traces of second discharge current are shown in Figure 6. The oscilloscope was triggered by the arc discharge. The first pulse represents the electrons from the arc arriving at the second discharge. The pulse following this is caused by the gas flow arriving from the arc discharge.

Relating the second discharge current traces to gas velocity is straightforward. Time-of-flight is interpreted as the time delay from initiation of the arc discharge to leading edge of the second discharge current pulse for the gas flow. For the trace of Figure 6A this is approximately 16 μs. Since the gas acquires a terminal velocity shortly after exiting the nozzle, flow velocity is assumed to be a constant over the distance between the two discharges. The terminal velocity is then just the discharge spacing divided by the time of flight for the gas flow. This terminal velocity, V_{max}, can be related to the heating temperature using the following equation [5]:

$$V_{max} = (\frac{2k}{k-1} RT_o)^{1/2} \tag{3}$$

where k is the ratio of specific heats,

R is the gas constant,

and T_o is the heating temperature. Once the temperature is determined, factors like arc voltage and capacitance can be changed to provide the optimum temperature for vibrational excitation.

Experiments were done to determine the heating temperatures for various arc capacitances and voltages. If arc capacitor voltages lower than 400 volts were used, arcing did not occur. Figure 7 shows the results of these experiments. It is obvious that by changing arc voltage, arc capacitance, or both, a desired heating temperature can be achieved. Higher arc energies produce lower gas temperatures. This seems to be caused by a superlinear increase in discharge volume with arc energy, thus reducing the energy per molecule.

To determine how effectively the gas is heated in the arc the energy given to the gas flow must be calculated. The energy given to the gas flow, E_{gas}, is given by

$$E_{gas} = \rho_0 \left(\frac{2}{1+k}\right)^{1/k-1} (\pi r_0^2) \left(\frac{2k}{k-1} RT_0\right)^{1/2} T_{arc} \left(\frac{3}{2} f_d + \frac{5}{2} \frac{1-f_d}{2}\right) (K_b T_0) \qquad (4)$$

where ρ_0 is the initial atomic density,

r_o is the radius of the nozzle throat,

K_b is Boltzmann's constant,

T_{arc} is the time duration of the arc discharge,

and f_d is the dissociated fraction. This equation calculates the rate at which gas particles leave the nozzle and multiplies this by the time duration of the arc and the energy per particle. The rate of particle flow is

calculated by multiplying the throat density by throat area and by throat velocity. To determine how much energy is deposited into the gas flow, one can do a rough sample calculation using the data for a 2 μf arc capacitor charged to 500 volts in this case. From Figure 7, a gas temperature of about 5000° K is produced in the arc. For an initial atomic density of 0.50 x 10^{19} cm^{-3}, the energy given to the gas flow, using equation 4, is 0.0013 joules. The energy stored in the capacitor is 0.25 joules. Thus, for this rough sample calculation, about .5% of the arc energy went into heating the actual gas flow exiting the nozzle. The remaining arc energy goes into heating gas in the reservoir, electrode heating, and resistive losses in the arc circuit. The effects of the magnetic field produced by the high currents in the discharge and electrodes were also calculated. The only effect of consequence was a possible slight increase in atomic density in the discharge region due to magnetic field pressure.

4. CONCLUSION

An experiment to produce vibrationally excited hydrogen has resulted in gas temperatures and densities calculated to be optimal for retention of vibrational energy in the gas flow. This flow of hydrogen gas can then be used in a second discharge for volume production of negative hydrogen ions. In the second discharge, the excited hydrogen would significantly increase H⁻ production due to the large increase in cross section for dissociative attachment. Work is presently being done to add a second discharge for volume H⁻ production to the source of vibrationally excited hydrogen.

REFERENCES

[1] Production and Neutralization of Negative Ions and Beams, 3rd Intl. Symposium, Brookhaven, 1983, New York, A.I.P. Conference Proceedings no.111, 1984.

[2] M. Allan and S. F. Wong, Effect of Vibrational and Rotational Excitation on Dissociative Attachment in Hydrogen, Phys. Rev. Lett., Vol. 41, p. 1791, 1978.

[3] J. M. Wadehra, Negative Ion Production via Dissociative Attachment to H_2, in Ref. 1, pp.46-53.

[4] W. P. Allis and H. A. Haus, Electron Distributions in Gas Lasers, J. Appl. Phys., Vol. 45, pp. 781-791, 1974.
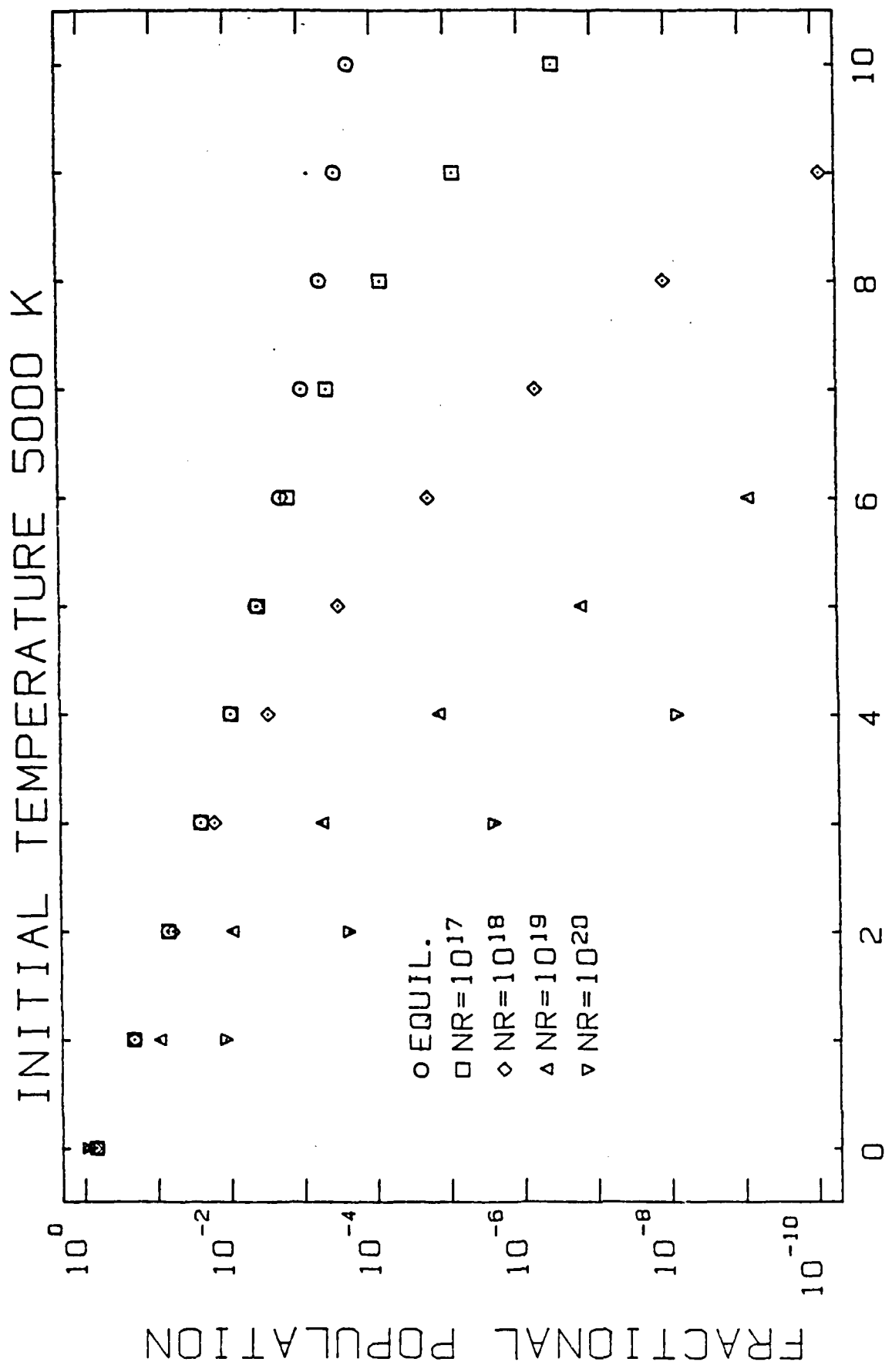
[5] A. H. Shapiro, The Dynamics and Thermodynamics of Compressible Fluid Flow, vol. I, The Ronald Press Company, New York, 1953, p. 73-105.
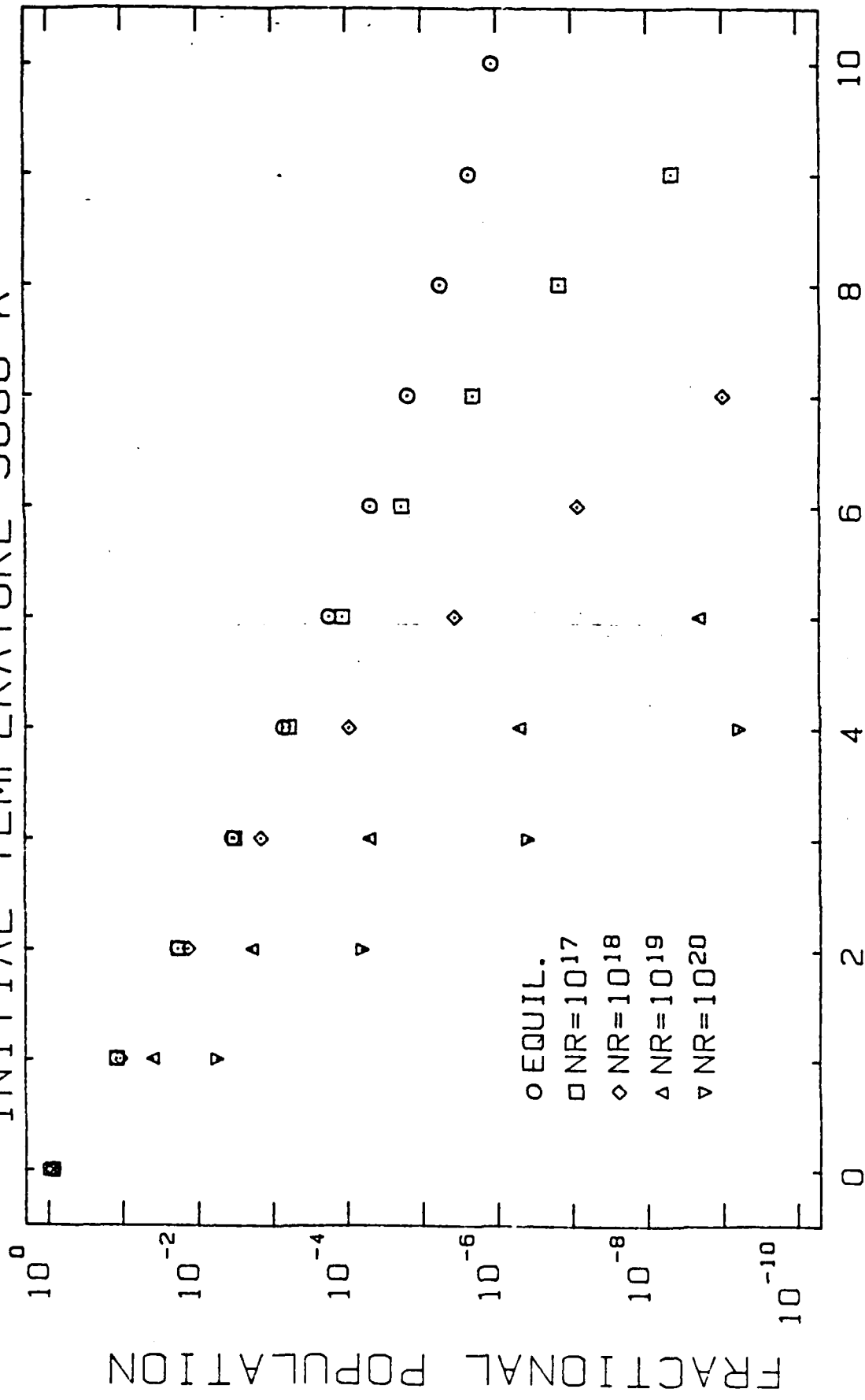
Figure 1. Vibrational state populations resulting from expansion of hydrogen heated to 3000 K. nr is the product of nozzle radius and molecular density. The Equilibrium curve is for a temperature of 3000 K.

Figure 2.   Same as 1 except 5000 K.
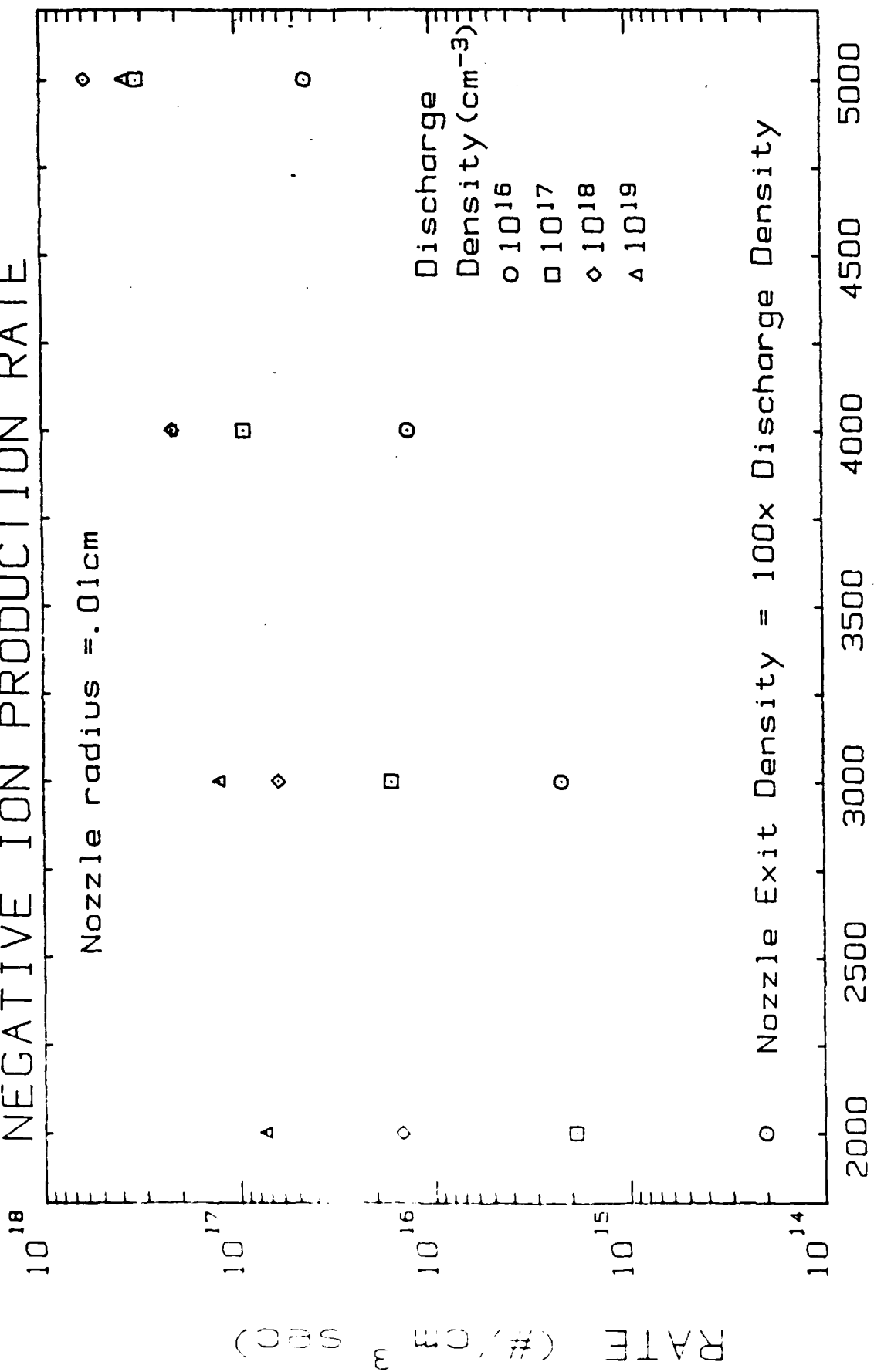
Figure 3. Negative hydrogen ion production rates for vibrationally excited hydrogen produced by the expansion of a heated gas.
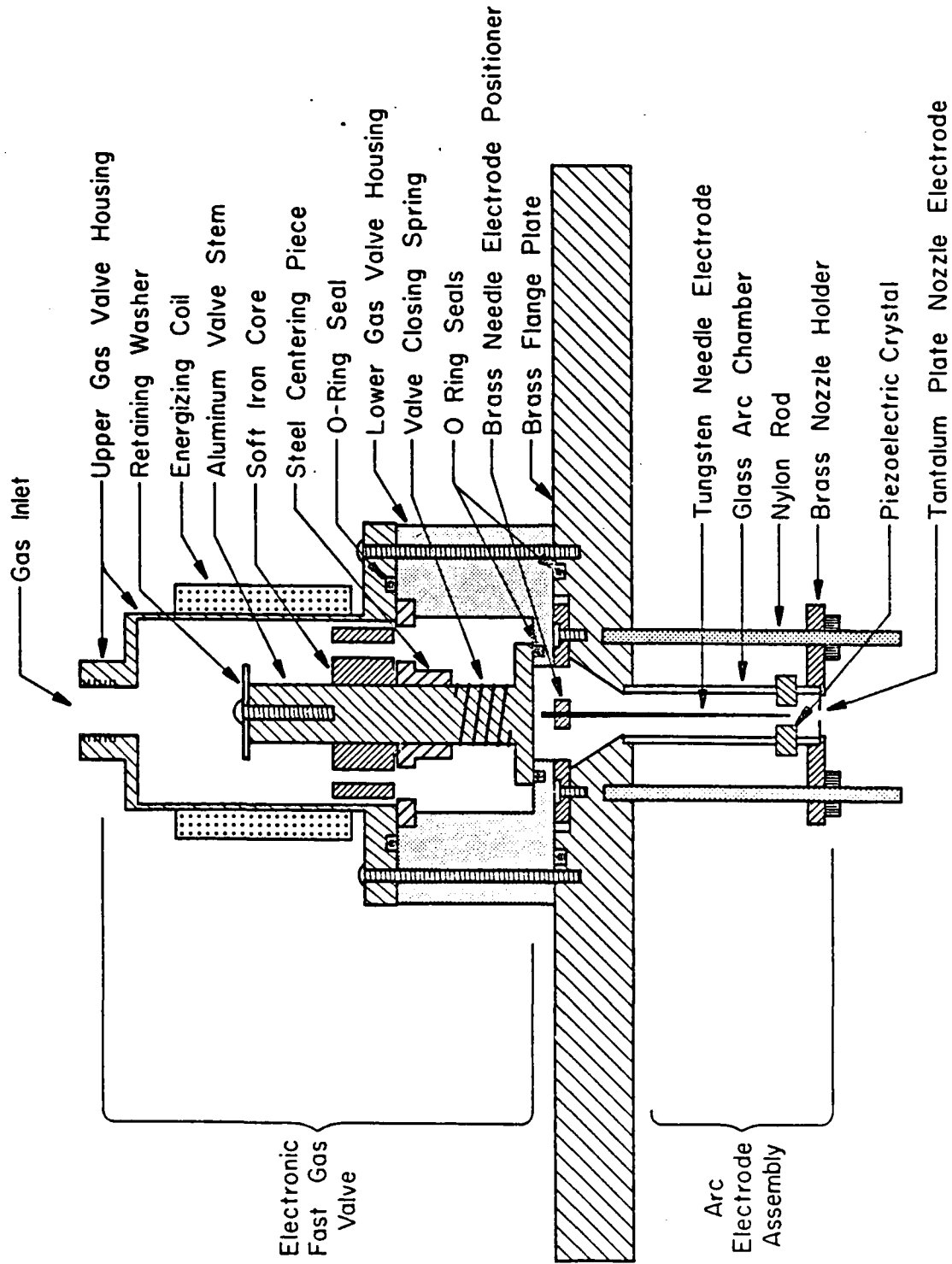
Figure 4. Cross-section of the electronic fast gas valve, arc chamber, and arc electrodes.
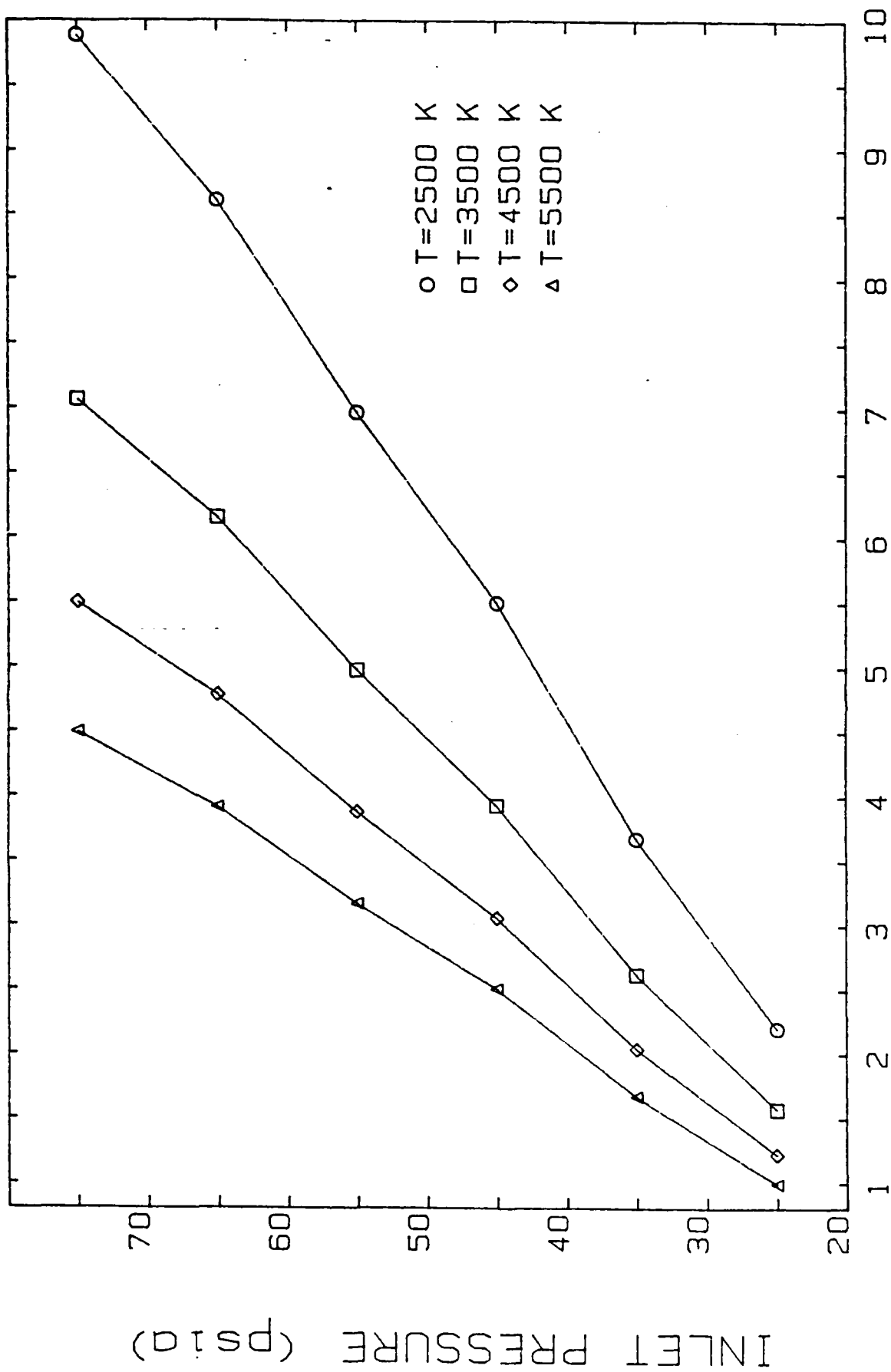
Figure 5. Valve inlet pressure vs. gas density in the arc discharge for various gas temperatures.

2nd Discharge Current Traces
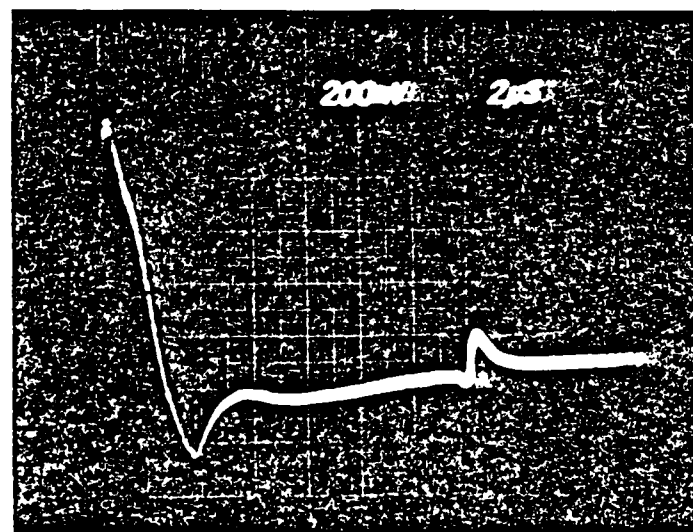

a) C = 2 μf,   V = 400v
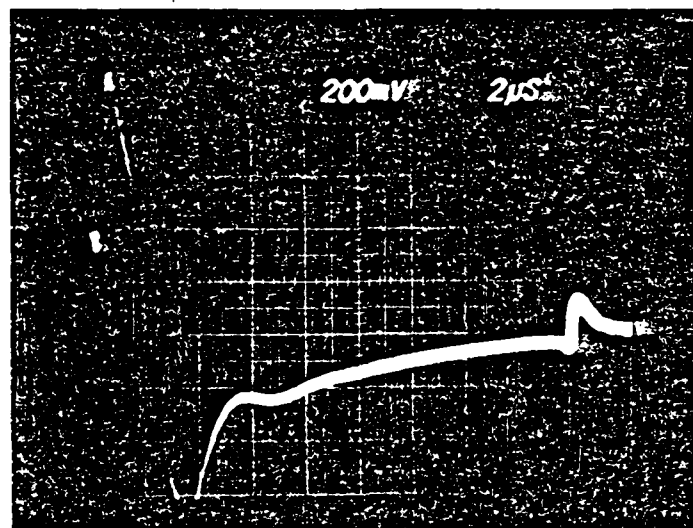
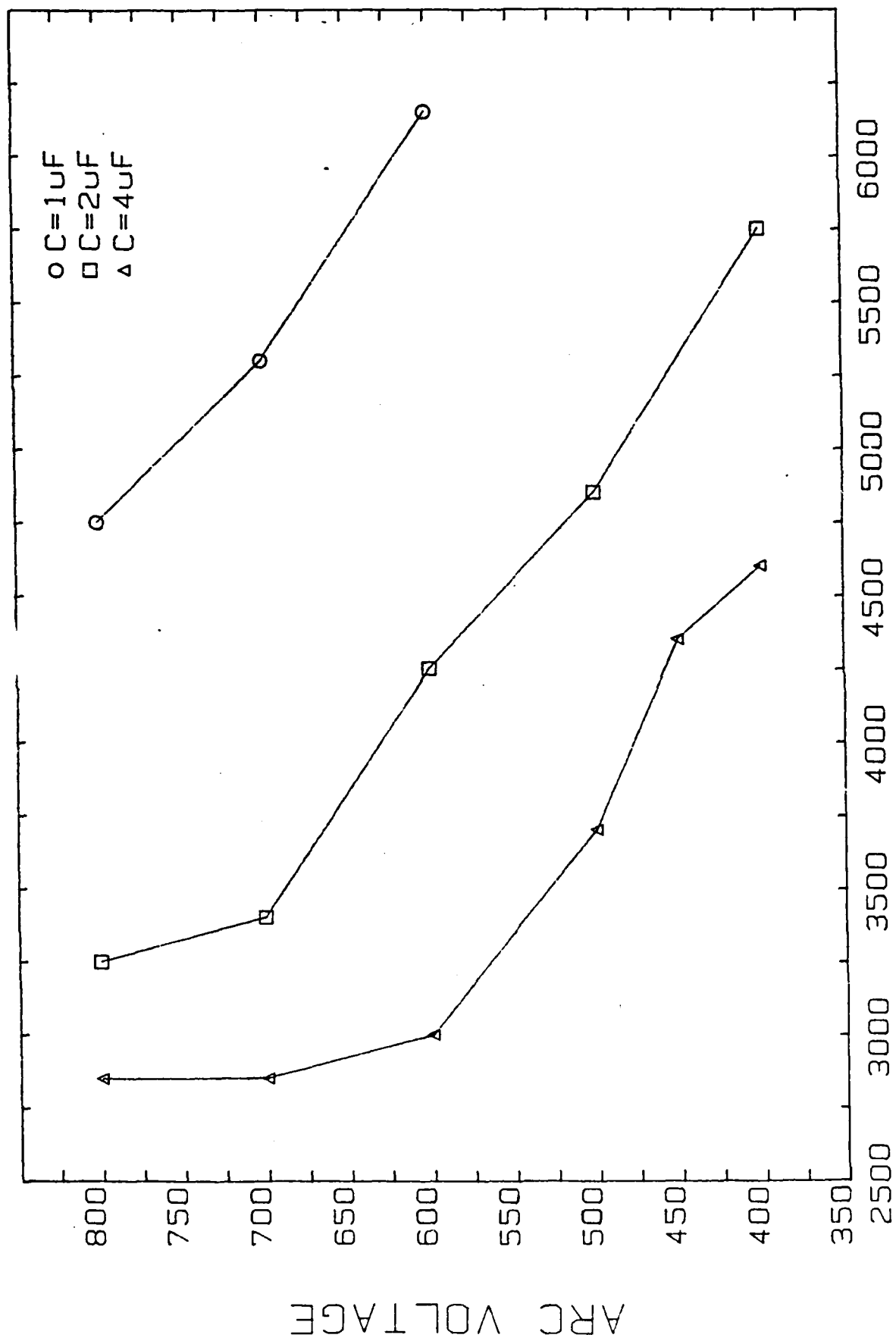b) C = 2 μf,   V = 600v

Figure 6.   Oscilloscope traces of second discharge current.

Figure 7.   Arc voltages vs. arc temperatures produced, for various arc capacitances.

V.   Construction of a System to Produce Negative Hydrogen Ions

1.   INTRODUCTION

The problem addressed in this section is the construction of the second discharge region in a two discharge system shown schematically in Figure 1. The first discharge is designed to heat hydrogen gas in such a way as to produce high vibrationally excited populations. The gas then flows through a nozzle and expands into the second discharge region yielding a low translation temperature while retaining its vibrational excitation.

The second discharge is to supply a large number of lower energy electrons (<4eV) to optimize the dissociative attachment process. The second discharge region must also include an extracting field for the extraction of H^- ions and electrons from the plasma. The extracted ions must then be separated from the electrons and collected to determine H^- density in the plasma.

The design and performance of the first discharge is detailed in a earlier section. Hydrogen gas is pulsed into the discharge using a fast electronic gas valve. Parallel to the average flow of the gas is a tungsten needle suspended perpendicularly over a tantalum disk which has a hole of radius R in the center of it that forms the nozzle. The discharge is initiated between the needle and the nozzle when the gas reaches the desired density N. The gas temperature is dependent on the arc energy which is determined by the capacitance and voltage applied to the needle-nozzle arc. Theoretical calculations presented earlier give the relative populations of the separate vibrational levels in the gas expansion as a function of gas temperature and of the product NR. In order to preserve most of the vibrational excitation, an upper limit of 10^{18} cm^{-2} is placed on the NR product. This NR product reflects the number of collisions taking place in the expansive flow. The stated limit keeps the vibrationally de-exciting collisions at a minimum. The gas temperature reflecting the vibrational populations was determined using time of flight measurements.

The focus of the work presented in this section is the ion producing plasma. The processes exploited for negative ion production are as described below. Conditions in the gas discharge for maximum ion production are examined. The experimental apparatus is described. Extracted data is characterized and compared to theoretical calculations.

Electron impact dissociative attachment is the dominant process for the production of negative hydrogen ions in an electrical discharge[1]. In this process, an electron is captured by an H_2 molecule forming an intermediate resonant state of H_2^- . The resonant state then dissociates into a negative hydrogen ion and a hydrogen atom. With the H_2 molecule initially in the ground state, the cross section for this process is very small[2]; 2.8×10^{-21} cm^2 with an electron threshold energy of 3.75 eV. It has been found experimentally[3] and theoretically[4] that the cross

section is greatly enhanced when the molecule is initially vibrationally and/or rotationally excited. Assuming an initial ground state configuration, the enhancement is approximately one order of magnitude for each vibrational state up to v=4, where v is the vibrational quantum number. There is also a reduction in the required threshold energy for each higher vibrational/rotational state. The enhancement for rotationally excited states is less dramatic where only an order of magnitude is calculated between J=0 and J=10, where J is the rotational quantum number.

It has been suggested[5], that the rate of negative ion production may be optimized under nonequilibrium electrical discharge conditions. The nonequilibrium conditions have associated with them relaxation times which are the times required for the various excited modes to attain equilibrium populations. The rotational relaxation time is short as it only takes a few collisions to equilibrate the rotational states. The vibrational relaxation times are longer allowing these modes to survive more collisions before equilibration. We must therefore produce a discharge supplied with high vibrational populations and low electron energies to achieve a large dissociative attachment rate.

A numerical solution[5] has shown that the maximum fraction of discharge energy channeled into dissociative attachment occurs when the discharge has an E/N ratio of about 40 Townsend (1 Td = 10^{-17} V-cm^2) where E is the electric field in V/cm and N is the neutral density in cm^{-3}. Most of the discharge energy goes to the excitation of the lower vibrational levels from the ground state and to dissociation. Their calculations also show that an increase in vibrational temperature leads to an increase in the fraction of discharge energy channeled into the dissociative attachment process. Other calculations[6] show that the distribution function with E/N = 30 Td has an abundance of low energy electrons. The average energy of the electrons for these conditions is calculated to be 1.4 eV.

2. DESIGN CONSIDERATIONS

There were many factors that had to be considered in the design of the second discharge region. The expansive flow of the gas from the nozzle had to be unobstructed. Obstructions would confine the expansion and increase the probability of de-exciting collisions. A fairly uniform E field in the discharge region with an E/N ratio of approximately 40 Td was desired. The discharge region had to be in close proximity to the nozzle to minimize the amount of de-excitation of the vibrational states.

We can estimate that the gas density goes something like $1/r^2$, so for a nozzle radius of .1 cm, the density drops by a factor of 100 when 1 cm away. This nonuniform density made the variability of the extraction point with respect to this distance important. Considering that 1550 torr exists at the nozzle, the pressure 1 cm away is about 15 torr. If we let the second

discharge's dimensions be 1 cm, the Paschen curve[7] for the
breakdown of hydrogen with pd≈15 torr-cm gives us a sparking
potential of 650 V. For 300 K, this gives an E/N of about 135
Td. An E/N ratio of 40 Td and a breakdown condition in the
discharge region could not simultaneously be accomplished so a
filament supplying primary electrons was called for.

The electrodes producing an adequate extractor field had to
be implemented in close proximity to the discharge region. The
extraction field had to be perpendicular to the average velocity
of the gas flow so as to not obstruct the flow with the
electrodes and support assembly. The extracted current would
contain both electrons and ions so an accelerating field,
magnetic separator, and collection points were required in the
extractor assembly. The extractor assembly had to be
electrostatically shielded from the first discharge, support
assemblies, and surrounding support circuitry. We also had to
shield the extractor assembly from the ambient gas to protect
from any unwanted discharges. Finally, the second discharge had
to fit the geometrical constraints of the first discharge
assembly, vacuum system, and of available parts.

3. DESIGN OF THE APPARATUS

3.1 SECOND DISCHARGE REGION

A parallel plate configuration was chosen for the geometry
of the discharge region as shown in Figure 2. Ease of
construction and implementation into the system as well as
availability of known breakdown data for this geometry were the
basis for this choice. The plates were orientated parallel to
the average velocity of the nozzle flow. The plate length in
this direction was 4 cm. The plate separation was .9 cm and a
width of 5 cm was chosen for uniform E field and relatively
unobstructed flow. The plate near the filament was a copper
screen of 45% transparency with a 2 × 15 mm slit near the nozzle
to maximize primary electron flow from the filament to the
discharge region. The screen was maintained at ground potential.
The plate on the extraction side of the discharge region was made
of copper sheet (1/32"). A .10" slot was centered in the plate
parallel to the flow allowing a variable extraction point along
the flow. Bounding the width of the discharge region were brass
support pieces which were maintained at ground potential. The
top of the discharge region was bounded by the brass nozzle
holder also at ground potential. The bottom of the region was
unbounded.

3.2 FILAMENT

The filament was a single strand of thoriated tungsten wire.
Its diameter was .010" and its length was 1.5 cm. It was
suspended parallel to the average gas flow about 2 to 4 mm from
the slit in the screen of the discharge region. The filament

wire was spot welded to thick nickel wires of diameter .0375"
which suspended the filament approximately 1.2 cm from a support
assembly made mostly of brass. The material directly behind the
filament was aluminum tubing. The normal operating temperature
of Th-W filaments is in the range of 1900-2100 K. An observed
saturated emissive current density suggested that we were in this
range. It was found that this high operating temperature had
detrimental effects on the system as a whole. Filament material
evaporated and collected on adjoining parts. Soldered
connections were melted. Plastic wire insulation was melted.
The problem was solved by providing a good thermal path out of
the vacuum. Ceramic standoffs in the filament support assembly
allowed good heat conduction as well as electrical insulation for
the assembly. The support assembly was attached to the large
brass plate containing the vacuum for maximum heat dissipation.
The support assembly was maintained at the filament's potential
to maximize the primary electron flow towards the discharge
region. The support assembly exhibited azimuthal symmetry with
respect to the axis determined by the filament's length to
provide a similarly symmetric electron flow.

A variable 60 Hz AC heating current was supplied to the
filament wire. The maximum heating current used was 8.4 A rms.
The heating current was slowly increased from zero to the maximum
setting on a time scale of about 2 seconds. An isolation
transformer allowed the filament's AC circuitry to float at a
desired DC potential. To maintain a constant potential at the
filament, the filament's DC potential supplying circuitry was
attached to the middle of a 10 ohm resistance shunting the
filament.

3.3 EXTRACTOR ASSEMBLY

The close proximity requirement of the nozzle and the
extraction point dictated the extractor assembly design. The
extraction point distance is defined as the distance from the
nozzle along the line determined by the average flow velocity.
The shielded assembly had to contain the extracting and
accelerating fields as well as the magnetic separator and
collection points. The available magnets allowed the minimum
extraction point distance of 1 cm from the nozzle end of the
slotted plate. Therefore, a gas expansion within a cone of about
25 degrees could survive to the extraction distance without any
wall collisions.

The electrode configuration, borrowed from electron
optics[8], was that of adjacent conducting cylinders as seen in
Figure 2. Each electrode was a thick copper disk with a hole in
the center. The disks were placed in succession along the axis
determined by the centers of the holes. The fields produced by
such electrodes exhibit axial symmetry along this axis. Although
the electric fields are not uniform, the fields do offer a
focussing action which could carry the electrons and ions a long
way without wall collisions provided that no other collisions

occur.   Insulation between the electrodes was provided by mylar disks of thickness .006".

A rough calculation showed that the potential along the axis between two semi-infinite electrodes would reach the electrode potential at a distance of 1 D from the plane of symmetry where D is the hole diameter.   It was assumed that a minimum disk thickness of approximately 2-3 D was required to prevent overlap of the extracting and accelerating fields.   To isolate the influence of the magnetic field from the accelerating E field and to allow sufficient electrode thickness for minimum field overlap, an overall length of the assembly from the extraction point to the magnets was determined to be 10 D. Geometrical constraints imposed by the first discharge and the magnets determined this length and a hole diameter of D = .070" (.178 cm) was decided upon.

The first electrode nearest the discharge region was in physical and electrical contact with the slotted plate.   A flat ridge on the disk matching the slot's dimensions was provided to make the slotted plate appear more like a uniform plane which would in turn produce a more uniform E field in the discharge region.   The ridge's length as well as the electrode's diameter was .5" (1.27 cm).   The electrode's thickness including the ridge was 2 D.   The second electrode's thickness was 3 D.   The E field produced between these two electrodes determined the extractor field.   The second electrode is also referred to as the extractor.   The third electrode, also known as the separator, provided the accelerating field in conjunction with the second electrode.   The original hole diameter in this electrode was maintained to a thickness of 3.5 D and then abruptly opened to a hole diameter of approximately 5.4 D (3/8") which was maintained for a thickness of 6 D.   The larger diameter region was provided to utilize the maximum amount of the magnet's cross section and to allow space for field fringing.   It was assumed that the larger volume and surface area would facilitate the diffusion and collection of the deflected electrons.   Terminating this region was a solid disk used to collect the H^- ions.   The collector disk was maintained at the separator's potential although electrically insulated.

Surrounding all of the electrodes was a hollowed cylinder of teflon which in turn was surrounded by a brass cylinder maintained at ground potential.   A slot along the length of the cylinders allowed access for the potential supplying circuitry. The brass cylinder and the magnets were supported by an aluminum stage whose adjustable height allowed a variable extraction point.

The magnets were bar magnets of unknown composition. Their dimensions were 1 x .5 x 1.9 cm.   The magnets were placed co-linearly, north to south, with a separation of 1.4 cm.   The field intensity produced was approximately parabolic along the line separating the two magnets.   The field across the cross section was fairly uniform.   A field intensity of about 400 Gauss existed within a distance of .2 cm from the center point between

the magnets. The maximum field nearer to the magnets was about 700 Gauss.

3.4 FIRST DISCHARGE DESIGN MODIFICATIONS

A brass housing of rectangular toroidal geometry was inserted between the electronic fast gas valve and the brass plate as seen in Figure 3. The inside diameter was designed to accept the existing brass needle support piece as well as provide room for electrical insulation from the brass plate, fast gas valve, and the housing itself. Insulation was provided by teflon pieces whose outside diameter matched the housing and whose inside diameter of .6" matched the fast gas valve's outlet. This forced all of the gas leaving the valve to be directed to the discharge region.

Connection to the needle's potential supplying circuitry was supplied by a 3/16" brass rod screwed into the edge of the needle's support piece. The rod entered the brass housing in a coaxial configuration through a 1/2" brass quick connect. The shielding coaxial configuration was maintained back to the box containing the potential supplying circuitry with brass tubing. Insulation between the rod and shield was provided by teflon.

The discharge region was shielded by a brass cylinder that fit the outside diameter of the brass nozzle holder. Tinned copper braid filled the gap between this shielding cylinder and the large brass plate. Stainless steel screws which supported the nozzle holder probably provided the return current path to the brass plate. The large brass plate which had a diameter of 6" was the ultimate ground of the overall system as it was connected to a nearby water pipe by a large tinned braid.

3.5 TIMING OF THE SYSTEM

The timing of events became important in this pulsed gas system. Identical conditions between trials was desired. The filament was allowed to warm up for a set period of time before the coil opening the fast gas valve was energized. The initiation of the first and second discharges at the desired densities was based on timing components rather in conditions present in the discharge regions. Data acquisition was made easier using timing pulses rather than triggering the oscilloscopes using the signals presented.

The system's timing sequence was initiated by the 60 Hz Variac used in conjunction with the filament's heating current supply. As the Variac was varied from zero to the desired setting, a half rectified signal was sent to a level detector which triggered a standard timer. The filament operated at its maximum heating current for about 3.5 seconds before the triggering of the SCR to energize the coil which opened the fast gas valve. A typical delay of 2.3 to 2.9 ms was observed before a measurable amount of gas reached the piezoelectric crystal in the first discharge region. The delay can be explained as the

time it takes for the rarefaction caused by the sudden presence of the evacuated discharge region to propagate through the H_2 supply line back to the tank. The H_2 supply consisted of a length of 1/4" polyflow tubing back to a regulator and supply tank. The supply line was 3.5 m in length and the speed of sound in H_2 at 15°C is 1.3×10^5 cm/s. Therefore, t=l/v=2.7 ms is in excellent agreement with the observed delay. About 3.5 s after the valve was opened, a triac in the filament's circuitry shut off the heating current to minimize sputtering of the filament by ambient gas.

The piezoelectric's output indicated a ramping effect until the pressure achieved and maintained its maximum value. The delay to maximum pressure typically was 250-500 microseconds. The gas pulse typically lasted about 30-50 ms. A level detector and timer triggered by the piezoelectric's output was implemented to trigger the SCR in the needle arc circuitry to initiate the first discharge when the pressure ramp hit its maximum value.

In the second discharge region, it was observed that the region between the filament and the screen broke down much earlier than the region between the parallel plates for higher pressures. To compensate for this, a timer controlling SCRs in the filament and slotted plate circuits dictated when the respective potentials would be simultaneously applied initiating the second discharge's breakdown.

4. EXPERIMENTAL RESULTS AND DISCUSSION

4.1 NEEDLE ARC DISCHARGE

When the first discharge was modified the nozzle was also replaced by a new one with a radius ten times larger (.1cm) to facilitate the desired density in the second discharge region. The pressure in the first discharge region was desired initially to be on the order of a few atmospheres. This is due to the fact that once a discharge is initiated, a high E/N ratio will channel most of its energy into dissociation of the hydrogen gas. Dissociation is undesirable as the dissociative attachment process is optimized with high densities of vibrationally excited H_2. A lower E/N ratio will have the inelastic collisions predominantly produce vibrational and rotational excitation of the gas producing the desired vibrational populations in the free expansion. This higher pressure would put us on the high pressure side of the Paschen minimum for hydrogen in the second discharge. The required potential for breakdown of the second discharge would be much too high to produce the desired high density of low energy electrons for the dissociative attachment process in the plasma sheath. The mean free path[9] between collisions of neutrals would also be so low that any H^- produced would not survive to the extraction region. To maximize this mean free path and to attain the optimal E/N in the second

discharge region, a pressure range of 1 to 5 psi absolute was used. Pressures stated in this paper are the backline pressures of the fast gas valve at room temperature. The new needle was longer, more tapered, and had a sharper point than the one previously used. This combined with the fact that a larger radius nozzle was being used, required a minimum breakdown voltage of 550 Volts compared to 400 Volts for the earlier configuration.

Because of the time scale of the measurements in the second discharge, it was desired to lengthen the 10 μs that the arc heated the gas. To accomplish this, a resistor was placed in series with the capacitor and needle to produce an RC time decay. A current transformer monitored the arc current. In this needle arc configuration, no measurable difference in the second discharge's behavior was observed except for small amplitude noise superimposed on the extractor and separator outputs and large amplitude noise at the H⁻ collector.

4.2 EMISSION CURRENTS FOR THE FILAMENT OF THE SECOND DISCHARGE

The filament was heated by a 60 Hz current of 8.4 A rms. Its value was chosen because the observed emission current increased steadily as the heating current was increased until it began to level off around this value. The filament was bright white. The filament's DC potential was maintained at -50 V with respect to the grounded screen in front of it. This potential reflects a maximum ionization cross section of H_2 by electrons[10]. The filament was observed to breakdown the gas about 50 μs before the discharge region when the pressures were 35 psi and up. No such early breakdown was observed for lower pressures. When the timer applying the DC potentials to the filament and slotted plate was triggered while gas was in the region, the emission current from the filament and to the slotted plate exhibited a hump resembling an overdamped oscillator before reaching a steady state value. To avoid this transient behavior, the timer was set to trigger the SCRs when the fast gas valve opened. Typical discharge currents from the filament were on the order of 25-50 mA. Varying the filament's had little effect on the discharge currents implying a space charge limited flow. The filament proved quite durable surviving about 1000 gas shots before needing replacement.

Typical emission currents from the filament and to the slotted plate were linear with respect to the potential of the slotted plate. The ratio of the emission current to the separator to that to the extractor was linearly proportional to the difference of the extractor (=separator) and slotted plate potentials. These linear relationships indicate that the current flow was not space charge limited.

4.3 EXTRACTOR CHARACTERISTICS

The electrodes in the extractor assembly were provided to

focus the beam of extracted ions and electrons to the separating magnetic field. The electrodes were designed to minimize loss to the walls. The potential and electric field configuration in this geometry obey a complex relation[11]. Calculations of the electric field along the axis of symmetry of the system indicate a maximum field of E(V/cm) = 7.5 times the potential difference between the two electrodes.

Breakdown in the extractor assembly is undesirable so the maximum allowed potential that could be applied to the extractor without breakdown occurring had to be found. The slotted plate was set at 5 V to minimize ionization in the discharge region while the primary electrons from the filament were present. Breakdown was observed with the extractor potential equal to 200 V for all pressures. So the maximum potential applied to the extractor or separator had to be less than 200 V. This put a damper on the desired ratio for proper focussing of the beam. To get around this, the extractor and separator were maintained at the same potential in hopes that the extractor field would also act as the accelerating field for the magnetic separator.

The discharge observed at 200 V with the primary electrons present may be explained by the high potential drawing the sheath formed by the ionizing collision of the primaries into the extractor tube. As the electrons of the sheath are drawn in, so will the ions by ambipolar diffusion. The decreased positive ion density leaves room for the neutrals to also diffuse into the tube. Continual recombination of the ions offers another source of neutral particles. The result will be a self sustaining discharge at the mouth and extractor field region of the extractor tube. There is also the possibility that some of the gas may have been adsorbed by the copper walls of the extractor tube. The high energy electrons may have stripped enough of the hydrogen off of the walls and ionized it to produce the observed currents.

4.4 SECOND DISCHARGE CHARACTERISTICS

The data were produced by varying the pressure between 1 to 5 psi in 1 psi increments and by varying the slotted plate's potential between 20 to 100 V in 20 V increments. For each slotted plate potential, the potential of the extractor and separator, tied together, was varied from the slotted plate's potential in 20 V increments to an arbitrary value, typically 40 V. Families of curves showing supposed H$^-$ collection were taken. The curves represent the voltage on the device side of the sampling resistor. A drop in voltage therefore implies current flow to the device.

The current to the slotted plate exhibited two regions. Negligible current was observed before any gas reached the discharge region. A small current typically on the order of 1 to 10 mA was observed in the region for a time period of 150 to 200 us. A larger current was then observed on the order of 4 to 10 mA which continued for times in excess of 2 ms. These typical

currents existed regardless of the extractor/separator potential.

Current to the H⁻ collector electrode was observed during the first 150-200 μs time period. The currents ranged from .4 to 2.4 μA. They generally increased linearly with pressure, the slotted plate's potential, and the potential difference between the extractor and the slotted plate. After the initial time period, the current was quenched to zero when the second discharge current was observed at the slotted plate. It is believed that this collector electrode current is due to negative hydrogen ions or to electrons produced by secondary emission in the separator region. With the 400 Gauss field in the separator region, only electrons with energies greater than say 1000 eV could reach the collector. Separator currents were not of the magnitude to shield the B field with the field produced by the current itself.

Typical extractor currents were in the range of 10 to 1000 μA and typical separator currents of 1 to 100 μA were observed for the above slotted plate ranges. The large slopes with respect to time indicate that these currents are from breakdown due to electron multiplication either in the discharge region or the extractor field region. The extractor and separator curves had the same shape indicating the same source of their currents. The discharge currents observed obeyed the following relations. The extractor, I_{ext}, and separator, I_{sep}, current maxima varied linearly with pressure. Also,

$$I_{sep}/I_{ext} = (.00129)V_{sl} + .0438 \quad \text{for } V_{sl}=V_{ext}$$

$$I_{ext}+ I_{sep} = (12.57)V_{sl} - 27.17 \quad \mu A$$

$$I_{sep}/I_{ext} = (.005)(V_{ext}-V_{sl}) + .09$$

where V_{sl} and V_{ext} are the slotted plate and extractor voltages respectively for the previously stated ranges. The discharge currents are believed to be due to an extracted beam of electrons and ions. If there had been gas in the extractor tube, electron multiplication would probably take place and a different relationship would exist. We therefore conclude again that the density in the extractor is negligible and that the extracted currents are electron-ion beams.

5. MODELING OF THE DISCHARGE REGION

5.1 NEUTRAL DENSITY IN THE DISCHARGE REGION

The temporal dependence of the slotted plate's discharge current indicates that the neutral density in the discharge region is a function of time. As described earlier, the piezoelectric crystal in the first discharge region indicated at higher backline pressures that the pressure was a function of time. It ramped up to a maximum value which it maintained for a relatively long time. Since the piezoelectric proved ineffective

at lower pressures, we model the density at the nozzle as having
a similar ramping time dependence. Since the discharge region
exhibited two discharge currents, we assume that the ramping
takes place during the first discharge current and that the
maximum density is maintained during the second discharge
current's time period. The pressure ramps up to its maximum
value 150 μs and the gas temperature is assumed to be 300 K.

We now consider the gas expansion in the discharge region.
Since negligible density is assumed in the extractor tube, we
assume that the gas opens up into a cone whose surface area does
not intersect the extractor hole. Assume that the gas expands
with an angle θ =10° as shown in Figure 4.

To model the density and temperature of an assumed ideal
gas within this cone, we consider the flow as being approximated
by a one dimensional isentropic flow through a passage of varying
cross section. The assumption of an expansion angle of 10°
supports the condition that the fractional rate of change of area
with respect to change in distance along the axis is very small
which is a condition for the one dimensional approximation. We
assume that the flow is supersonic which is reasonable
considering that we have a gas expanding through a hole into a
vacuum.

Working tables of isentropic flow[12] give information
concerning the gas as it expands to larger areas. We consider
the maximum density at the nozzle to take on the value of 3 psi
at 300 K with nozzle radius R=.1 cm. The initial velocity of
sound in the gas is 1.3×10^5 cm/s which is also given to be the
velocity through the nozzle during expansion ie, Mach# = 1. At
the extractor, 1.1 cm down the flow, the tables give us that the
gas velocity is about 2×10^5 cm/s. The time of flight is 5.5 μs.

To relate the observed emission currents to the observed
first discharge currents, we now approximate the gas flow cone to
uniformly take on the properties of the flow at z=.7 cm. This
distance corresponds to the midpoint of the filament. The width
of the cone at this point is d=.44 cm. We approximate the cone
as rectangular box having the filament's length (1.5 cm) and a
square cross section of $(.44 \text{ cm})^2$. The filament's emission
current reaching the discharge region is approximated as a planar
source.

5.2 H⁻ PRODUCTION RATE

We will continue to use the model of the neutral gas density
in the discharge region. The current density to the slotted
plate will be calculated using the area of the rectangular box
used earlier in consideration of the current multiplication
relationships. To determine H⁻ production however, we will
examine the neutral density parameters in the cone at the
distance corresponding to the entrance of the extractor tube.
The electric fields used for calculations will be set equal to
the slotted plate's potential divided by the plate separation
because after the onset of ionization, the plasma's parameters

will be determined by the more uniform E field offered by the parallel plates.

At the extractor tube where z=1.1 cm, the tables for isentropic flow give us that n/n_o= .0342 and T= 78.6 K where n_o is the density corresponding to 3 psi at 300 K. The same ramping time dependence for the density is assumed. Observations of the families of curves indicate that H⁻ production does not begin until after the 50 μs needed to build up the first discharge current. We use t=50 μs as the origin for H⁻ production and don't consider times after the H⁻ current is quenched by the second discharge at 150 μs.

To calculate H⁻ production rates, we need the ratio n_e/N where n_e is the electron density. For a given time, an E/N ratio is calculated using the appropriate values of E and N from the stated relations and the electron drift velocity as a function of E/N. The electron density is calculated utilizing the appropriate first discharge current, I, the area of the rectangular box (.44 x 1.5 cm), and the appropriate drift velocity in the relation n_e = (I/eAv). The n_e/N ratio is then calculated and the effective rate of H⁻ production is found using Figure 5, assuming T_g=100 K which is the gas temperature. The effective rate, based on the work of Garscadden and Bailey, is that due to H⁻ production in a 40 Td discharge including contributions from all vibrational levels. The results of these calculations are that the production rates are about 10^{15} cm⁻³/s for H⁻.

Observation of the E/N values indicate that we are near the 40 Td value. The fractional discharge energy deposited into dissociative attachment is nearly constant from 30 to 100 Td, so the rates calculated as compared to those for a 40 Td discharge will probably be of the same order of magnitude. The calculated rate of H⁻ production is given by the following relation.

$$dN^- = n_e N k_{DA} = Ct^{ex} \qquad t \text{ in } \mu s$$

Table 1 lists these coefficients as well as an average dN⁻/dt production rate. The calculated rates as function of time are approximately parabolic owing to the linear dependence of the neutral density with time and the nearly linear dependence of electron drift velocity versus E/N.

Table 1   dN⁻/dt -versus- Time
Calculated Coefficients and Average Rates

V_{sl}(V)	C(cm⁻³/s)	ex	dN⁻/dt(cm⁻³/s)
20	.187×10¹¹	1.384	1.04×10¹⁵
40	3.38	1.826	1.49
60	1.79	2.108	3.00
80	1.59	2.254	5.33
100	5.18	2.260	4.89

5.3   H⁻ DENSITY IN THE PLASMA

Using the H⁻ production rate and the extracted current, we want to calculate the expected H⁻ density in the plasma.   We consider a cylinder as an extension of the extractor tube into the cone of the neutral gas flow.   Assume a uniform neutral density in the cylinder.   Assume zero net flux of all species to the surface area of the cylinder inside the cone except for the circles formed by the intersection of the cone and the cylinder. We assume that $N^- << n_e = N^+$ to allow the H⁻ to freely diffuse while not under the influence of the space charge field produced by ambipolar diffusion of n_e ard N^+.

A rough calculation with $V_{sl} = 40$ V gives the electron mobility to be on the order of 10^5 cm²/Vs while the positive and negative ion mobilities are on the order of 10^3 cm²/Vs.   Assuming equal density gradients, space charge neutrality, and characteristic energies for the electrons and ions as 1.7 and 1 eV respectively, solution of the 3 specie one dimensional diffusion equations in a parallel plate configuration give the space charge electric field E_s(V/cm)= 5.8 cot($\pi x/L$).   Here L is the plate separation (.9 cm) and x is the distance to the plate. A distance of .2 cm from the parallel plates gives this field as 7 V/cm.   A distance of .1 cm from the plate containing the extractor hole is only 16 V/cm.   So the assumption of a small field due to ambipolar diffusion holds.

5.3.1   LOSS RATE PROCESSES

Now that we have the production rate of negative hydrogen ions in the above cylinder, we wish to examine some of the destruction or loss rate processes occurring.   If we assume a steady state concentration of negative ions in the cylinder, the production rate must equal the loss rate, ie.

$$dN^-/dt = N^-(1/t_1 + 1/t_2 + 1/t_3 + \ldots)$$

Here t_1, t_2, etc. represent the lifetimes of the negative ions due to the respective loss processes.   A loss process with a long lifetime for the H⁻ ions implies that a high concentration of H⁻ exists for a given production rate.   A short lifetime would indicate that the H⁻ ions are being destroyed frequently and a lower density would therefore exist.

These loss rate processes are usually represented by a rate constant which is an average of a product of a cross section with a velocity.   The dimensions are cm³/s.   Multiplying this rate constant by the concentration of the H⁻'s collision partner in the process yields the lifetime for the process.   Since our product rate is on the order of 10^{15} cm-3/s and we assume that $N^- << n_e$ where n_e is about 10^9 cm⁻³, we are looking for lifetimes of less than 10^{-6} s to balance the above equation.

One loss rate process is the possibility of collision with a positive ion, H^+, producing two neutral hydrogen atoms. This process known as mutual neutralization has a rate constant[13] of approximately 2×10^{-7} cm^3/s. Wherein our positive ion density is on the order of $3-9 \times 10^9$ cm^{-3}, the product of these gives a lifetime on the order of $1.6-.6 \times 10^{-3}$ s. This lifetime is too long considering the calculated production rate and therefore could be neglected.

Another possible loss process is that of the ion colliding with a water molecule to produce a H atom and an OH^- ion. The rate constant for this reaction[14] at room temperature is 3.7×10^{-9} cm^3/s. Many measurements were made on humid days in the summer. The overnight pumpdowns of the system were 4×10^{-7} torr. Even if we assume an atmosphere entirely of water molecules, the lifetime presented is 4×10^{-4} s.

Another destruction process is that of associative attachment where a hydrogen atom and a negative hydrogen ion collide to produce a vibrationally excited H_2 and an electron. This reaction is important when the relative energy is less than .75 eV. The rate for this reaction is 1.8×10^{-9} cm^3/s at room temperature[15]. Using transport coefficients, we can determine the rate of dissociation as a function of E/N and time. Multiplying this rate by the electron and neutral densities present give us a dH/dt rate. The average dH/dt values calculated for slotted plate voltages of 20-100 V are on the order of $1-585 \times 10^{16} cm^3/s$. Multiplying these rates by the full 150 μs time period gives us H densities formed by this process on the order of $1.5-877 \times 10^{12} cm^{-3}$. The calculated lifetimes are on the order of $50-1.9 \times 10^{-6}$ s. Again this lifetime is quite long with respect to the calculated production rate but is getting more in the range that we expect for loss rates.

Since we assume the negative ions capable of free diffusion, we used the diffusion length for a parallel plate geometry which is $\Lambda = L/\pi$ where L=.9 cm. The reduced mobility[16], K_o, for H^- in H_2 at these E/N ranges is about 40 cm^2/Vs. The average reduced pressure, p_o, for this model is about 3 torr and the mobility under these conditions is found from the relation: $K = K_o(760/p_o) = 1.0 \times 10^4$ cm^2/Vs. Assuming a characteristic energy of 1 eV for the negative ions, gives $t_d = 8 \times 10^{-6}$ s, the diffusion lifetime to the walls.

Taking the minimum lifetime process which is associative attachment having t=1.9 μs and taking the minimum production rate of 10^{15} cm^{-3}/s gives us a negative hydrogen ion density of 1.9×10^9 cm^{-3}. This seems too high considering the average calculated electron densities are only $3-8 \times 10^9$ cm^{-3}. Not included yet in these loss rates is that of stripping of the H^- by electrons having energies in excess of the electron affinity of .75 eV. Finding the electron characteristic energy as a function of E/N gives us a time averaged range of .83-2.95 eV. The electrons do have enough energy to strip the ions and a large enough electron density is present to make this loss process substantial. We have also neglected other loss processes such as

neutralization by the other positive hydrogen species or impurities present.

5.3.2 EXTRACTED ION CURRENT

Another way to get an idea of the negative ion densities present in the plasma is to relate them to the extracted currents using the following relation[17],

$$J_s = eN^-(\kappa T_e/m_-)^{1/2}$$

where J_s is the saturated extracted negative ion current density and T_e is the electron temperature. If we assume that the neutral density extends into the extractor tube up to the point where the extractor field exists, we can include diffusion to the walls of the extractor tube. We assume diffusion in the radial direction only and the solution is the familiar Bessel function density distribution. We assume in the following that all of the ions reaching the extractor field make it to the collector plate. The ion velocities are found using the electron's characteristic energy. Equating the extracted current to the sum of the collected current and that lost to the walls by diffusion gives us densities of $4-8 \times 10^6$ cm^{-3}. *The calculated velocities are on the order of 10^6 cm/s.* The 400 Gauss field in the magnetic separator requires ions with velocities of 3.8×10^6 cm/s to survive deflection to the collector electrode. This assumes a Larmor radius of 1 cm. This velocity would represent a 7.5 eV ion. For electrons this represents energies in excess of 1 keV. We therefore conclude that the observed collector current is due to H$^-$ ions. It is assumed that the minimum required energy for the ions could easily be picked up while passing through the sheath. Also, the extractor potential in many cases exceeded that of the slotted plate by 20 to 40 V. The extracted ions could have easily attained the required energy here.

6. DISCUSSION

The calculated densities using the different methods differ by 3 orders of magnitude. The nonuniformity of the neutral flow made approximating the E/N ratio difficult. This nonuniformity of density in addition to the fact that we had a flowing gas also makes valid use of the various rate constants questionable. Conditions in the plasma of the second discharge region were certainly not those assumed in the ideal case presented in the theoretical calculations of the production rate.

To explain the 3 orders of magnitude gap, we must examine some of our assumptions. We neglected heating of the neutrals in our model. As the neutrals passed by the filament of their way downstream to the extractor region, their density was relatively high. For lower E/N ratios, more energy is deposited into vibrational excitement of the gas. This energy could then be channeled into translational energy which manifests itself as an

increase in "temperature". Had the gas temperature been 300 K rather than the assumed 100 K, the rate of H^- production would drop one order of magnitude for the same amount of fractional ionization.

If the discharge current density had been incident on the whole parallel plate's area rather than onto that assumed in the calculations, then the electron density and therefore the fractional ionization would decrease by a factor of 20. This would be manifested in a decrease in the rate of H^- production by one order of magnitude.

If we examine the ratio of the separator to the extractor currents for emission and breakdown, we see that the separator current is approximately one order of magnitude less than the extractor current. If we assume that the H^- current has the same relation for collection on the various electrodes, then the observed H^- collector current would imply a plasma density of one order of magnitude greater than that calculated by the extracted current equation. If we further assume that the same relation exists for the ratio of the extractor current to that collected on the walls of the electrode that was maintained at the slotted plate's potential, then we can say that the observed collector current implies a plasma density two orders of magnitude greater than that calculated by the extracted current equation.

This would put the H^- density in the plasma in the 10^7-10^8 cm^{-3} range. The dominant loss processes would therefore be associative attachment, diffusion to the walls, and probably stripping by electrons. The lifetimes of these loss processes would be in the 10^{-6}-10^{-7} s range. Not included in these calculations is a diffusive loss along the gas flow which could be great as the neutral density is a strong function of distance along the flow and so should be the plasma parameters.

REFERENCES

1. J. R. Hiskes, J. de Phys., 40, C7-179(1979).

2. G. J. Schulz and R. K. Asundi, Phys. Rev., 158, 25(1967).

3. M. Allan and S. F. Wong, Phys. Rev. Lett., 41, 1791(1978).

4. J. M. Wadehra and J. N. Bardsley, Phys. Rev. Lett., 41, 1795(1978).

5. A. Garscadden and W. F. Bailey, Progress in Astronautics and Aeronautics, 74, 1125(1980).

6. H. Brunet and P. Vincent, J. Appl. Phys., 50, 4700(1979).

7. M. J. Schonhuber, IEEE Trans. Power Aprt. Sys., PAS-88, 100(1969).

8. V. K. Zworykin, G. A. Morton, E. G. Ramberg, J. Hillier, A. W. Vance, Electron Optics and the Electron Microscope, John Wiley & Sons, Inc.,New York, 378 (1945).

9. L. B. Loeb, Fundamental Processes of Electrical Discharge in Gases, John Wiley & Sons, New York, 646 (1939).

10. D. Rapp, P. Englander-Golden, J. Chem. Phys., 43, 1464(1965).

11. V. K. Zworykin, et. al., Op. cit., p. 382.

12. A. H. Shapiro, The Dynamics and Thermodynamics of Compressible Fluid Flow, The Ronald Press Co., New York, (1953).

13. J. T. Moseley, W. Aberth, and J. R. Peterson, Phys. Rev. Lett., 24, 435 (1970).

14. D. L. Albritton, Atomic Data and Nuclear Tables, 22, 1(1978).

15. F. C. Fehsenfeld, C. J. Howard, and E. E. Ferguson, J. Chem. Phys., 58, 5841 (1973).

16. E. Graham, D. R. James, W. C. Keever, D. L. Albritton, and E. W. McDaniel, J. Chem. Phys., 59, 3477 (1973).

17. A. Guthrie and R. K. Wakerling, The Characteristics of Electrical Discharges in Magnetic Fields, McGraw Hill, New York, (1949).
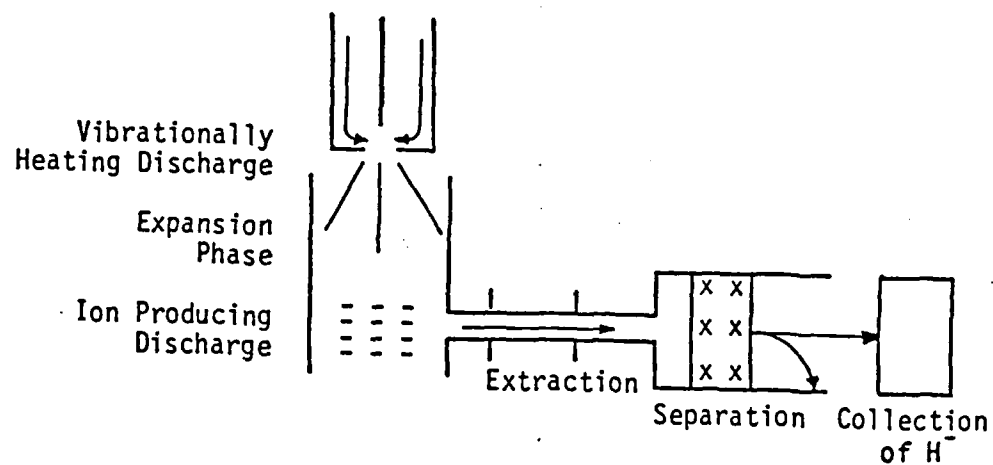
Figure 1. Schematic diagram of two discharge negative hydrogen
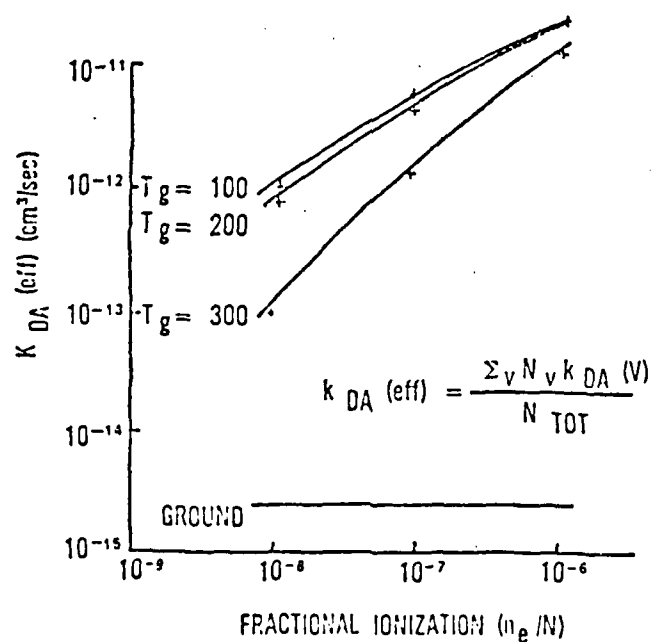ion source utilization vibrationally excited hydrogen.

$$k_{DA} \text{(eff)} = \frac{\Sigma_V N_V k_{DA} (V)}{N_{TOT}}$$

FRACTIONAL IONIZATION (n_e/N)

Figure 5. Effective rate constant of H^- production including all
vibrational levels as a function of fractional ionizationn
and gas temperature. Discharge conditions of 40 Td are
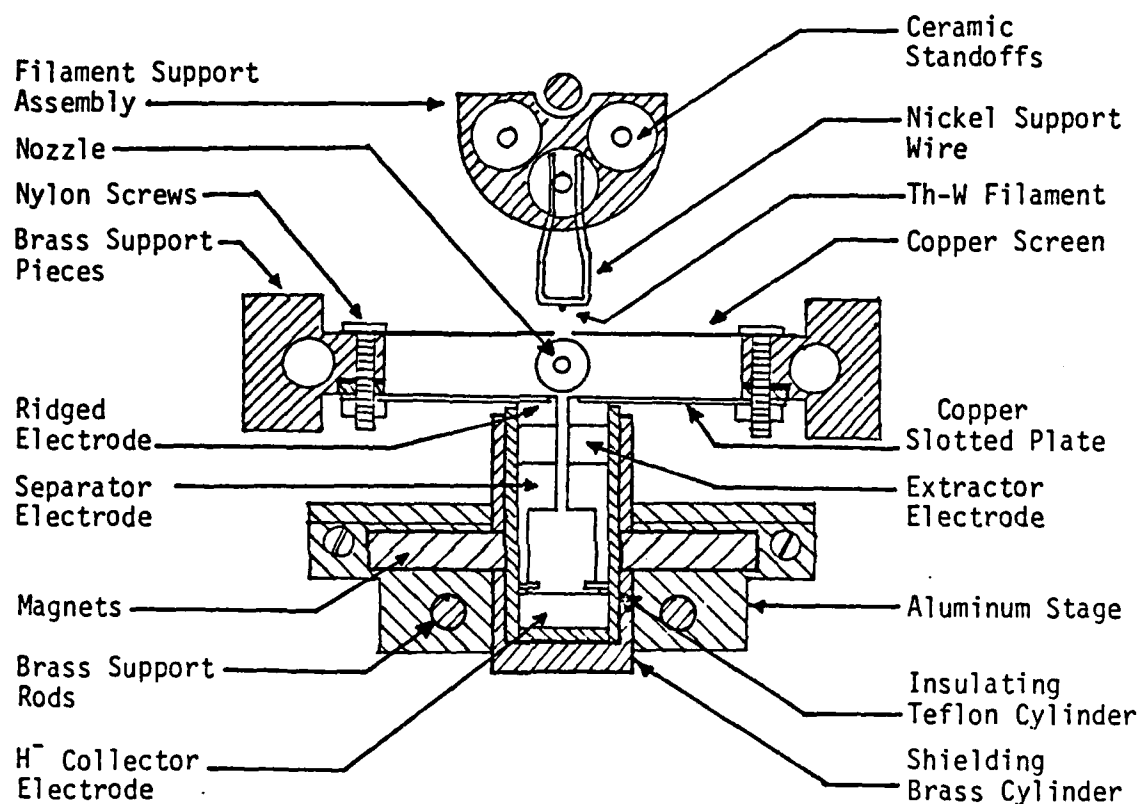assumed. (after [5]).

Figure 2. Top view of second discharge region including extraction, separation, and collection electrodes. Gas flow is out of the nozzle and then into the paper. A partial side view is shown in Figure 4.
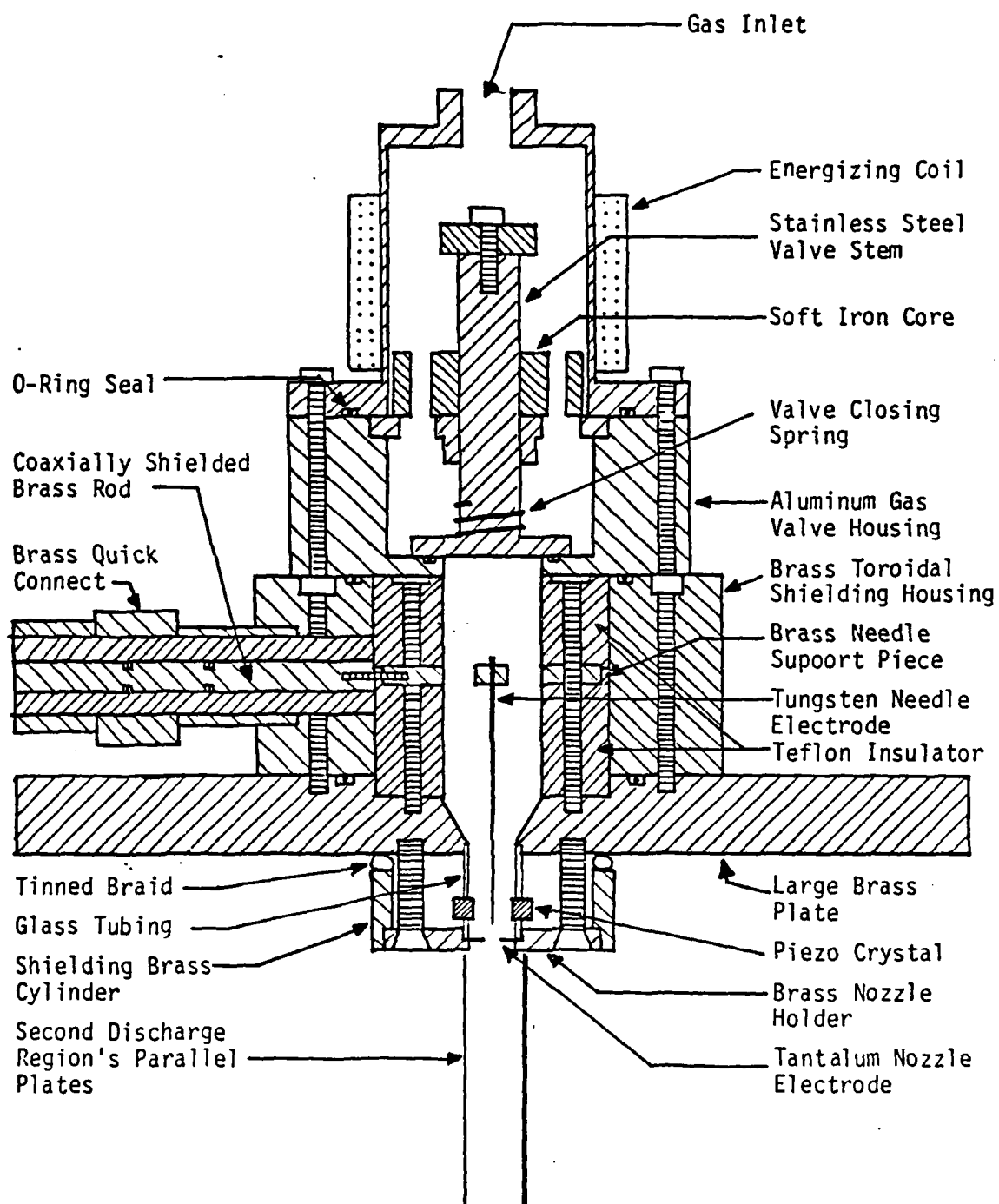
Figure 3. Side view of modified first discharge assembly including fast gas valve and part of second discharge region.
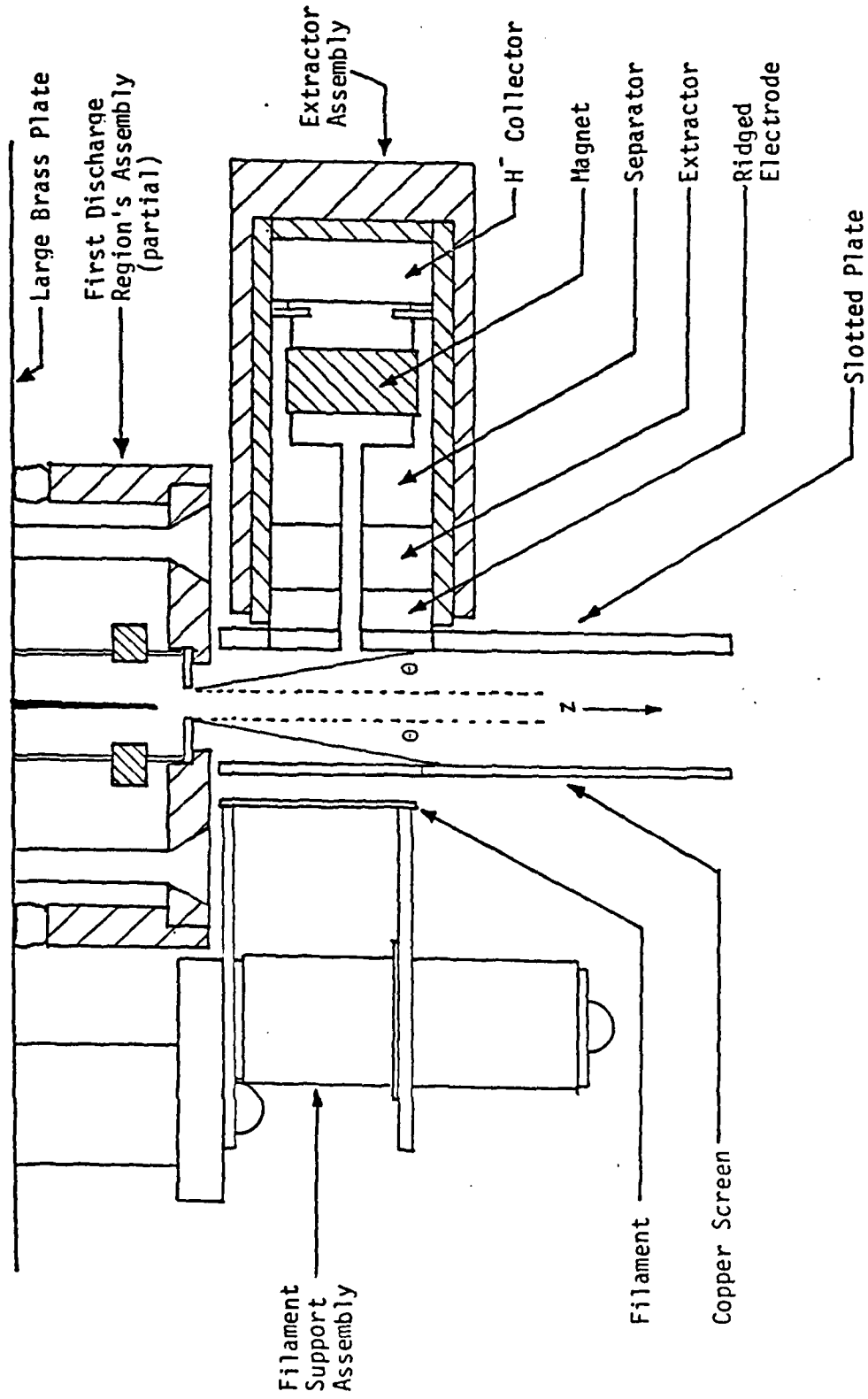
Figure 4. Side view of first and second discharge regions. Included are filament assembly, extractor assembly, and model of neutral gas flow cone.

Written Publications

"Indirect heating od solid hydrogen with a moderately powered laser", J. L. Guttman & R. J. Turnbull, Journal of Applied Physics, 58, 170(1985).

"Fabrication of planar and cylindrical solid hydrogen pellets for laser interaction experiments", J. L. Guttman & R. J. Turnbull, Review of Scientific Instruments, 55, 1941(1984).

"Generation of vibrationally excited hydrogen for use in a negative ion source", R. J. Turnbull, S. R. Walther & J. L. Guttman, Proceedings, 3rd International Symposium on the Production and Neutralization of Negative Ions and Beams, Brookhaven, A.I.P. Conference Proceedings Number 111, 132(1983).

"Production of Vibrationally excited H_2 for use in an H^- Source", S. R. Walther & R. J. Turnbull, (submitted for publication)

"Construction of a System to Produce Negative Hydrogen Ions", P. W. Genis & R. J. Turnbull, (in preparation)

Professional Personnel Associated with the Research Effort

    R. J. Turnbull, Professor
    F. R. Ore, Research Engineer
    J. L. Guttman, Research Assistant
    S. W. Walther, Research Assistant
    P. W. Genis, Research Assistant
    V. E. Scarpine, Research Assistant

Degrees Granted

    Ph.D. in Electrical Engineering, October 1982 to J. L. Guttman, Thesis: Laser Heating of Solid Hydrogen for Production of Vibrationally Excited Molecules for use in Negative Hydrogen Ion Sources.

    M.S. in Electrical Engineering, May 1984 to S. W. Walther, Thesis: Production of Vibrationally Excited Hydrogen by Electrical Discharge Heating for use in a Negative Hydrogen Ion Source.

    M.S. in Electrical Engineering, January 1986 to P. C. Genis, Thesis: Construction of a System to Produce Negative Hydrogen Ions.

END DTIC

9 - 86